RSC Advances



REVIEW

View Article Online
View Journal | View Issue



Cite this: RSC Adv., 2024, 14, 7940

Recent advances in photoelectrochemical platforms based on porous materials for environmental pollutant detection

Shiben Liu, Jinhua Zhan ** and Bin Cai **

Human health and ecology are seriously threatened by harmful environmental contaminants. It is essential to develop efficient and simple methods for their detection. Environmental pollutants can be detected using photoelectrochemical (PEC) detection technologies. The key ingredient in the PEC sensing system is the photoactive material. Due to the unique characteristics, such as a large surface area, enhanced exposure of active sites, and effective mass capture and diffusion, porous materials have been regarded as ideal sensing materials for the construction of PEC sensors. Extensive efforts have been devoted to the development and modification of PEC sensors based on porous materials. However, a review of the relationship between detection performance and the structure of porous materials is still lacking. In this work, we present an overview of PEC sensors based on porous materials. A number of typical porous materials are introduced separately, and their applications in PEC detection of different types of environmental pollutants are also discussed. More importantly, special attention has been paid to how the porous material's structure affects aspects like sensitivity, selectivity, and detection limits of the associated PEC sensor. In addition, future research perspectives in the area of PEC sensors based on porous materials are presented.

Received 19th January 2024 Accepted 21st February 2024

DOI: 10.1039/d4ra00503a

rsc.li/rsc-advances

1. Introduction

Over the past few decades, global population growth and industrial development have resulted in serious environmental

School of Chemistry and Chemical Engineering, Shandong University, 250100 Jinan, China. E-mail: bin.cai@sdu.edu.cn

pollution.^{1,2} Substantial amounts of harmful chemical compounds, such as heavy metal ions, antibiotics, pesticides, and phenolics, have been discharged into the environment. The self-purification capacity of natural water bodies cannot cope with these increasing environmental pollutants, posing a severe threat to both the ecological environment and public health.^{3,4} These contaminants can be identified using traditional



Shiben Liu

Shiben Liu received a PhD degree from the Ocean University of China in 2022 before he joined the School of Chemistry and Chemical Engineering at Shandong University as a post-doc. His scientific interests are devoted to the fabrication of multifunctional porous materials for photoelectrochemical applications.



Jinhua Zhan

Jinhua Zhan received his BS degree in chemistry from Northeast Normal University, and his PhD degree from University of Science and Technology of China under the direction of Professor Yitai Qian in 2000. After two years' postdoctoral experience in Professor Chung-Yuan Mou's group at Taiwan University, he joined the National Institute for Material Science (NIMS) as a Researcher under the direction of Professor

Yoshio Bando from 2003 till 2006. In 2006, he joined the School of Chemistry and Chemical Engineering as a Professor at Shandong University. His current research has focused on nanomaterials for environmental sensing and remediation.

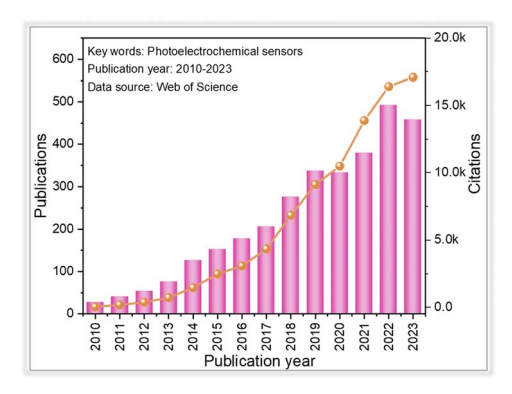


Fig. 1 Overview of the research contributions in photoelectrochemical sensors since 2010.

detection techniques like high-performance liquid chromatography, atomic fluorescence spectroscopy, atomic absorption/emission spectrometry, and inductively coupled plasma mass spectrometry. For However, the aforementioned detection techniques are limited by the large experimental instruments, specific operating conditions, and high training costs. Therefore, it is crucial to develop efficient techniques for the sensitive identification of these environmental contaminants.

Recently, photoelectrochemical (PEC) detection methods, as a branch of electrochemical (EC) detection techniques, have gained much attention in the field of tracing environmental pollutants, ¹²⁻¹⁵ which can be seen from the number of publications since 2010 (Fig. 1). Compared with conventional electrochemical detection techniques, the PEC method is based on the photo-induced electron-hole pair redox properties, which make it possible to generate signals (photocurrent). ¹⁶⁻¹⁸ Since light and photocurrent are employed as the excitation source and identification signal, respectively, a PEC sensor handles relatively lower background noise and higher sensitivity than those of conventional electrochemical detection methods due to the difference in the energy form of the excitation source and the converted electrical signal. Moreover, the PEC sensor is not directly in contact with the measured object, resulting in less

influence from the measurement condition.¹⁹ These advantages contribute to the simplicity of instrumentation, low cost, and ease of miniaturization associated with the PEC detection method.^{20–23}

In a typical PEC sensing system, the incoming light is regarded as the excitation source, and the electrical signal is used as the detection signal. 18,24,25 When exposed to light, the electrode containing the photoactive material is excited, resulting in the generation of photogenerated electron-hole pairs, which are subsequently transferred to the electrode surface. Cathodic photocurrent results from the electrons on the condition band (CB) being trapped by electron acceptors (A); otherwise, the holes on the valence band (VB) transfer to the surface of photoactive materials, where they react with the electron donors (D) to form anodic photocurrent (Fig. 2A).¹⁷ According to the different generation processes of the photocurrents at the interface between the electrode and electrolyte, the PEC detection sensors can be classified into two categories: (1) the analytes serve as electron donors or acceptors to directly react with photoactive materials;26,27 (2) the electrodes are first modified by recognition elements, after which the target concentration is determined through indirect physicochemical interactions between the targets and the recognition elements (Fig. 2B). For the commonly used recognition elements used in the PEC detection system, they can be divided into three categories: (1) aptamers refer to single-stranded synthetic nucleic acid molecules (DNA or RNA);28-30 (2) antibodies, which are mainly proteins, can be used as recognition elements to bind with target antigens such as proteins, toxins, and pathogens;31 (3) enzymes are biological catalysts that can bind to and act upon specific substrates.32

As can be seen from the inset above, whether the recognition element is contained or is free on photoelectrochemical sensing platforms, photoelectrochemical detection performance of a fabricated electrode is mainly determined by three factors, including light absorption capacity, photogenerated charge carrier separation and transportation within photoactive materials, and the transfer of surface charge carrier to the detection species.³³ To achieve excellent detection activity with



Bin Cai

Bin Cai obtained his PhD from Technische Universitat Dresden under Prof. Alexander Eychmuller in 2017. He then continued his career as a postdoc at Massachusetts Institute of Technology with Profs. Yuriy Roman and Yang Shao-Horn, and Pacific Northwest National Laboratory with Drs Chun-Long Chen and James De Yoreo. In 2020, he joined the School of Chemistry and Chemical Engineering as a professor at Shandong Univer-

sity and his current research interest focuses on nanocrystals, electrochemistry and analytical chemistry.

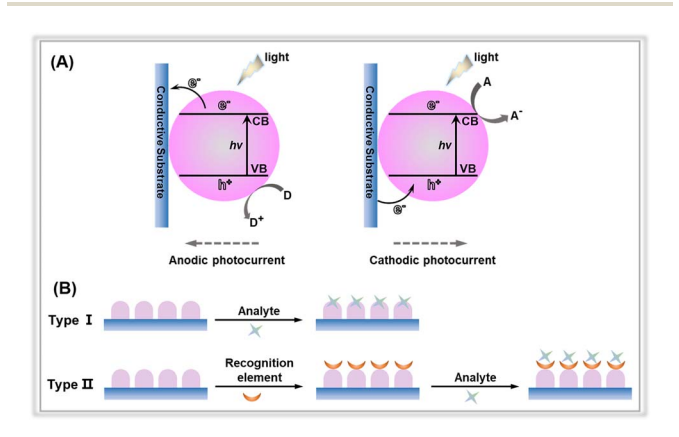


Fig. 2 (A) Anodic and cathodic photocurrent generation mechanisms of photoactive material-based electrodes. (B) Different types of PEC sensors with or without the recognition elements.

RSC Advances Review

PEC sensors, researchers have focused on exploiting various sensing devices and detection modes, and the design engineering of photoactive materials. Much effort has been directed towards reducing costs and simplifying the device fabrication for versatile and portable PEC sensing platforms. For instance, in some detection devices, capacitors and digital multimeters are utilized to output electrical signals instead of electrochemical workstations.34-36 Another area of research involves exploring different detection patterns, such as split-type detection, self-power detection, visual detection, and highthroughput detection. Despite extensive efforts in designing detection devices and modifying detection modes, the primary focus in constructing PEC platforms has been on investigating photoelectrodes. 19,37 To date, significant effort has been devoted to the development of photoactive materials as electrodes for PEC sensors. These materials include metal oxides, metal organic frameworks, graphene and carbon nitride.38,39

In recent years, porous materials have received considerable attention owing to their high surface area, relatively low density, large accessible space, and variable chemical composition. 40-42 Research interests in the applications of porous material-based PEC sensors were rapidly increasing, particularly in the field of determining environmental pollutants. 43 Due to their unique structure, porous materials are preferred over bulk materials for photoelectrochemical determination of environmental contaminants. As illustrated in Fig. 3, the porous material has a structural influence on the three factors governing the PEC detection activity of the sensor.

- (1) Light absorption capability: porous materials with small pores enable the incident light to penetrate their pore walls and scatter intensely inside the pore channels, thereby greatly improving the light harvesting ability of the porous materials.⁴⁴ Further, the feasible modifications of the band structure of the porous materials by altering the pore diameter also promote light absorption, particularly in the visible light region.
- (2) Photogenerated charge carrier separation and transport efficiency: the photoelectric conversion efficiency of a photoelectrode depends on the separation and transport of photogenerated charge pairs within the photoactive material. In the case of bulk materials, photogenerated charge pair separation

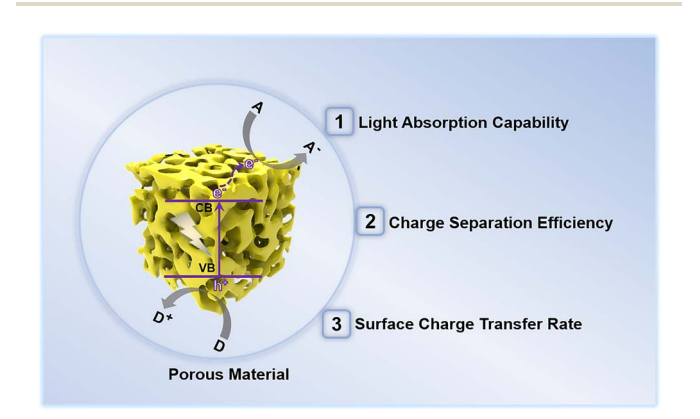


Fig. 3 Structural effects of photoactive porous materials on the performance of photoelectrochemical detection of environmental pollutants.

normally occurs in the space charge layer and the adjacent layers, leading to easy recombination. However, for porous materials, the charge separation and migration paths can be shortened due to their unique porous structures, ⁴⁵ enabling efficient photogenerated charge transfer within porous materials.

(3) Surface charge carrier transfer rate: porous materials possess a large specific surface area, which is advantageous for mass transfer during the photoelectrochemical detection. In addition, the exposed surface areas with abundant active sites provide sufficient functional groups conducive to interaction with recognition elements or direct trapping of the probe species. Hence, porous materials exhibit rapid surface charge carrier transfer rates and reaction kinetics.

Thus, photoelectrochemical sensing platforms based on porous materials have remarkable detection capabilities against environmental contaminants. This can be attributed to several factors, including enhanced light absorption, high photogenerated charge carrier separation and transport efficiency, and rapid surface charge carrier transfer rates during photoelectrochemical detection. As a result, these platforms offer a wide linear range, low detection limits, high sensitivity, excellent selectivity, and outstanding stability.

Recently, a significant number of reviews on PEC detection sensors for environmental pollutant determination have been published. 11,16,46-50 However, these studies focused on strategies for fabricating PEC detection systems and identifying the multiple contaminants, neglecting to discuss the effect of the presence of porous materials on the detection activity of PEC sensors. For instance, in 2020, Shu et al. provided a comprehensive summary of current research in photoelectrochemical sensing, with a particular emphasis on material design and engineering to regulate photoelectrochemical sensing performance. They also discussed photoelectrochemical sensing devices and detection modes.33 In another review by Li and coworkers, the central theme was a comparative analysis of electrochemical detection and photoelectrochemical detection, specifically addressing the question of which analytical method is more effective for tracing environmental pollutants.11 Further, in 2021, Yan et al. provided a concise overview of the fundamental and research progress of functional materials (such as metals, metal oxides, inorganic 2D materials, and carbon nanomaterials) in electrochemical and photoelectrochemical technologies for monitoring environmental pollutants.⁵¹ Despite these efforts, few reviews have focused on the relationship between the structure of porous materials and the detection activity of associated PEC sensors. So, in this review, we seek to thoroughly investigate the recent advancements in porous materials for environmental contaminant detection. Indeed, porous materials encompass a wide range of different types. Here, we specifically focus on photoactive porous materials, including but not limited to metal oxides, metal-organic frameworks (MOFs), covalent organic frameworks (COFs), graphitic carbon nitride (g-C₃N₄), and MXene (Table 1). We extensively discuss the structural effects of porous materials on the performance of PEC sensors. Finally, we propose the main challenges and future prospects of porous

Table 1 Typical photoactive porous materials for the photoelectrochemical monitoring of environmental contaminants

Photoactive porous materials	Common preparation method	Advantages
Metal oxides	Anodic oxidation, chemical bath deposition, hydrothermal	Suitable $E_{\rm g}$, fast surface kinetics
Metal-organic frameworks	Hydrothermal, slow evaporation and diffusion, iono-thermal, microwave-assisted, mechanochemical, electrochemical, sonochemical, microemulsion	Unique porosity, adjustable light response range
Covalent organic frameworks	Hydrothermal, ionothermal, microwave- assisted, sonochemical, mechanochemical, light-induced processes	π -electron conjugation, low $E_{ m g}$
Graphitic carbon nitride	Chemical exfoliation, thermal oxidation	Metal-free nontoxic, visible light responsive
MXene	Etching method	Small diffusion barrier, high conductivity

materials in the realm of PEC detection sensors. However, due to the space limitations of this review and the widespread use of porous materials in the field of PEC detection sensors, many intriguing and significant studies may not have been addressed. We apologize for any inadvertent omissions and appreciate the valuable contributions of all researchers in this field.

2. Photoactive porous materials

2.1. Metal oxides

Metal oxides play a crucial role in the field of photoelectrochemical sensing. 52,53 Indeed, there is a large body of research focusing on porous metal oxides for PEC sensing, which is difficult to categorize in a simple way, so here we only present some representative porous metal oxides, in particular semiconductor metal oxides (Table 2). Among all the porous metal oxides applied in PEC sensing, TiO2 has always occupied a unique position. 54-59 In addition, PEC detection sensors have been constructed using ZnO, SnO₂, WO₃, and Fe₂O₃ (ref. 60-65) (Table 3). For instance, in a study by Tavella and co-workers, a porous TiO2 array modified titanium electrode was constructed for PEC sensing of dopamine.66 The as-prepared electrode performed well for dopamine and has a wide response range (200~1500 μM) and a low detection limit (20 μM). In addition to nanoarrays, nanotubes also have a large number of pores. For instance, Fan et al. prepared a BiOI nanoflowers/TiO2 nanotubes (BiOI/TiO2) composite through a hydrothermal method (Fig. 4A and B).67 Due to the presence of porous

Table 2 Features of different metal oxides used in the fabrication of photoelectrochemical detection platforms

Photoactive metal oxides	Band gap/eV	Preparation method
${ m TiO_2}$	3.0~3.3	Anodic oxidation, hydrothermal, sol-gel
ZnO	3.7	Electrodeposition, hydrothermal, chemical bath deposition
SnO_2	$3.6 \sim 4.0$	Hydrothermal, electrospun
WO_3	2.8	Hydrothermal, solvothermal, co-precipitation
Fe_2O_3	2.2	Electrodeposition, hydrothermal

nanotube structure, the BiOI NFs/TiO2 NTs electrode provided more spaces for anchoring the aptamer, and thus the PEC platform demonstrated a significant activity for atrazine determination with a low detection limit of 0.5 pM (Fig. 4C and D).

Similarly, Wu et al. developed a PEC sensor for chlorpyrifos (CPF) detection based on bismuth sulfide nanoparticles decorating TiO₂ nanotubes with oxygen vacancies (Bi₂S₃/V₀-TNTAs), which realized a rapid photocurrent response to CPF within a linear range of 0.07~3.0 μM.68

In addition to the porous TiO2 nanomaterials, other photoactive porous metal oxides (ZnO, SnO₂, WO₃, and Fe₂O₃) have also exhibited excellent photoelectrochemical detection activity towards environmental pollutants. In a study by Wu and coworkers, CdS nanocrystals were decorated on porous onedimensional (1D) ZnO nanorods through a pulsed electrodeposition technique.69 The resulting CdS/ZnO hybrid photoelectrode was employed for PEC detection of the heavy metal ion, Cu²⁺. The porous ZnO nanorods provided an enlarged surface area for the dispersion of nano-sized CdS nanocrystals, thereby enhancing the photogenerated electron transfer via the "1D electron highway". The CdS/ZnO composite electrode demonstrated an ultrasensitive LOD of approximately 3 nM within a wide linear range of 0.01~1000 μM. Meanwhile, Velmurugan et al. prepared a WO₃/CuMnO₂ p-n heterojunction composite and applied it for "signal-on" PEC sensing of nitrofurazone.70 Porous WO3 nano-tiles were synthesized via a hydrothermal method and coupled with CuMnO₂ nanoparticles by an evaporative impregnation method. The porous WO₃ provided abundant surface sites for interaction with CuMnO₂ nanoparticles. Further, a p-n heterojunction was formed between the p-type CuMnO2 and the n-type WO3, which promoted photogenerated electron transfer due to the presence of a built-in electric field.71 As a result, the PEC nitrofurazone sensing performance of the WO₃/CuMnO₂ composite electrode demonstrated a wider detection range of 0.015~32 μM with a lower LOD of 1.19 nM, compared to pure CuMnO₂ nanoparticles.

α-Fe₂O₃ is a well-known visible light active semiconductor with a band gap of 2.2 eV, making it suitable for applications in PEC sensing. In 2019, Adhikari et al. prepared a Bi₂WO₆/α-Fe₂O₃ heterojunction photoelectrode by depositing porous α-Fe₂O₃

RSC Advances

Table 3 Metal oxide-based photoelectrochemical detection sensors for tracing environmental contaminants^a

Working electrode	Analyte	LOD	Linear concentration range	Ref.
NiCo-LDHs/TiO ₂ TNAs	Cr(vi)	0.12 μΜ	0.5 μM~1.8 mM	55
CdSe/TiO ₂ TNAs	Cd^{2+}	0.35 nM	1 nM∼10 mM	72
Fe ³⁺ /ZnO-Ag	Hg^{2+}	0.1 nM	0.5 nM∼100 nM	60
WO ₃ /Au	Hg^{2^+}	2.0 pM	4.2 pM∼840 pM	61
Fe ₂ O ₃ -CdS	Cu ²⁺	0.5 nM	50 nM~600 μM	73
ZnO-CdS	Cu^{2+}	3 nM	$0.01~\mu M{\sim}1~mM$	69
CdS/ZnO	Cd^{2^+}	3.3 μM	0.01 mM~5 mM	74
BiOI/ZnO NRs	Pb^{2+}	7.5 μ M	10 μM~100 μM	75
MIP@TiO ₂ NTAs	Perfluorooctane sulfonate	86 ng mL^{-1}	$0.5~\mu\mathrm{M}{\sim}10~\mu\mathrm{M}$	76
CdS/MnO ₂	Paraoxon	0.017 ng mL^{-1}	$0.05 \text{ ng mL}^{-1} \sim 10 \text{ ng mL}^{-1}$	77
TiO ₂ TNAs/CdS	Bisphenol A	0.5 pM	1 pM∼100 pM	78
SnO_2	Bisphenol A	1.2 nM	2 nM∼500 nM	79
MoS_2/ZnO	Propyl gallate	12 nM	0.125 μM~1.47 μM	80
TiO ₂ array/Ti	Dopamine	20 μ M	0.2 mM~1.5 mM	66
CdS QDs/TiO ₂ TNAs	Asulam	$4.1~\mathrm{pg~mL}^{-1}$	$0.02 \text{ ng mL}^{-1} \sim 2.0 \text{ ng mL}^{-1}$	57
BiOI/TiO ₂ NTAs	Atrazine	0.5 pM	1.0 pM∼600.0 pM	67
Bi ₂ S ₃ /V _o -TNTAs	Chlorpyrifos	6 nM	0.07μ M \sim 3.0 μM	68
$GQDs/TiO_2$ TNAs	Chloramphenicol	57.9 pM	0.5 nM∼100 nM	81
WO ₃ /CuMnO ₂	Nitrofurazone	1.19 nM	$0.015~\mu M{\sim}32~\mu M$	70
Bi_2WO_6/α - Fe_2O_3	Tetracycline	0.3 μΜ	$0.01~\mu M{\sim}25~\mu M$	63
P(33DT-co-3TPCA)/[BMIM]Cl-ZnO NRs	Aflatoxin B1	0.058 ng mL^{-1}	$0.10 \text{ ng mL}^{-1} \sim 10 \text{ ng mL}^{-1}$	82
rGO/TiO ₂ TNAs	Microcystin-LR	0.5 fM	1.0 fM∼500 fM	83
Cu ₂ O/TiNTs	Sulfide	0.6 μΜ	1 μM~300 μM	84
SnO ₂ -AuNPs	Nitrite	0.48 nM	1 nM~100 μM	85

^a MIP: molecularly imprinted polymer; NTAs: nanotubes; NRs: nanorods; V_o-TNTAs: TiO₂ nanotube arrays with oxygen vacancies; TiNTs: TiO₂ nanotube arrays; GQDs: graphene quantum dots; P(33DT-co-3TPCA): poly(3,3'-dithiophene-co-3-thiophenecarboxylic acid); [BMIM]Cl: 1-butyl-3-methylimidazolium chloride.

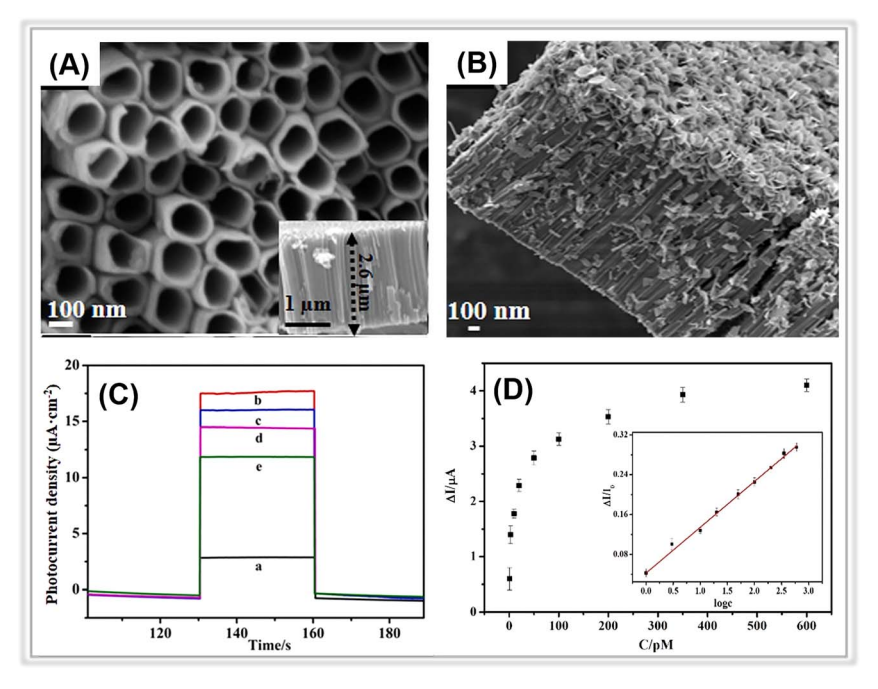


Fig. 4 SEM images of (A) TiO₂ NTs and (B) BiOI NFs/TiO₂ NTs. (C) Photocurrent responses of (a) TiO₂ NTs, (b) BiOI NFs/TiO₂ NTs, (c) aptamer/BiOI NFs/TiO₂ NTs, (d) BSA/aptamer/BiOI NFs/TiO₂ NTs, and (e) atrazine/BSA/aptamer/BiOI NFs/TiO₂ NTs. (D) Photocurrent change against atrazine concentrations. Adopted from ref. 67. Copyright 2021, with permission of Elsevier.

layers on the Bi_2WO_6 nanoflakes.⁶³ The influence of the $\alpha\text{-Fe}_2O_3$ layer thickness on the PEC detection activity of tetracycline was thoroughly investigated. After introducing porous $\alpha\text{-Fe}_2O_3$ layers,

the photocurrent of the hybrid composite-based photoelectrode increased (4.3 μA cm $^{-2}$) compared to that of pristine Bi_2WO_6 (1.2 μA cm $^{-2}$). Under optimized conditions, the photoelectrode

demonstrated a LOD of around 0.3 μM in the range from 0.01 μM to 25 μM . Hence, PEC sensors based on porous metal oxides hold great potential for tracing environmental contaminants.

2.2. Metal-organic frameworks

Metal–organic frameworks (MOFs), which are potential porous materials composed of transition metal ions and organic ligands, have attracted much attention in the area of environmental pollutants determination. MOFs, particularly photosensitive MOFs, have many potential applications in PEC sensing due to their inherent characteristics, such as permanent porosity, chemical stability, and unique optical properties. The Zeolitic Imidazolate Framework (ZIF), Materials Institute Lavoisier frameworks (MILs), Universitetet i Oslo (UiO), copper(II) benzene-1,3,5-tricarboxylate (Cu-BTC), and porphyrin-based MOFs (PCN) series MOFs have been extensively investigated for PEC sensing applications against hazardous pollutants (Table 4). MOFs

2.2.1. ZIF. The ZIF family of MOFs has been widely employed in the fabrication of PEC detection sensors. Among them, zeolitic imidazolate framework-8 (ZIF-8), a typical member of MOF materials, is composed of zinc ions and 2-methyl-imidazole ligands. ZIF-8 possesses excellent stability in aqueous conditions. More importantly, ZIF-8 exhibits porous structures and has the ability to generate abundant reactive species under light irradiation. These unique properties make it suitable for constructing PEC detection platforms for environmental pollutant determination. For instance, Chen et al. prepared a ZIF-8/ZnIn₂S₄ (ZIF-8@ZIS) photoelectrode for PEC detecting tetracycline (Fig. 5A). In this detection system, the porous ZIF-8, with plenty of active Zn(II) sites, could interact rapidly and specifically with the tetracycline, resulting in quenched photocurrent due to the swift transfer of

photoelectrons. The lowest detection limit calculated for the ZIF-8@ZIS PEC sensor was *ca.* 0.1 pM (Fig. 5B and C). In addition, it exhibited exceptional speediness, high stability, and strong selectivity during PEC monitoring of tetracycline.

2.2.2. MIL. Similar to the ZIF series MOFs, the MIL series MOFs have also been utilized in PEC detection. Recently, NH₂-MIL-125(Ti), a titanium-based metal organic framework (Ti-MOF) derived from the Ti metal ions and NH₂-BDC ligands, has exhibited excellent visible light absorption ability and stable redox reaction properties.96 In 2021, Yang et al. developed a molecularly imprinted NH2-MIL-125(Ti)/TiO2 compositebased photoelectrochemical sensor for oxytetracycline detection.97 The NH₂-MIL-125(Ti)/TiO₂ hybrid composite was synthesized via a simple solvothermal method, and then a molecularly imprinted polymer (MIP) was modified as a recognition element. The photocurrent of the MIP@NH2-MIL-125(Ti)/TiO2-modified electrode was significantly enhanced (0.8 μ A) compared to that of the MIP@TiO₂ (0.1 μ A), owing to the improved visible light absorption capacity and wellmatched band levels of the two components. As a result, the MIP@NH2-MIL-125(Ti)/TiO2-based photoelectrochemical detection sensor demonstrated a wide linear detection range from 0.1 nM to 10 µM, with a LOD of 60 pM.

2.2.3. UiO. UiO series MOFs have also demonstrated excellent photoelectrochemical detection activities against environmental contaminants. For instance, UiO-66 is composed of the $Zr_6O_4(OH)_4$ cluster and terephthalic acid. In 2021, Feng *et al.* synthesized $[Ru(bpy)_3]^{2+}$ @Ce-UiO-66/Mn:Bi₂S₃ composites and utilized them to construct aptamer-based PEC sensors for ofloxacin (OFL) detection.⁹⁸ Ce-UiO-66 MOFs were obtained by doping UiO-66 with Ce-elements. The cycling of Zr^{4+} – Zr^{3+} and Ce^{4+} – Ce^{3+} in porous Ce-UiO-66 enhanced charge separation efficiency. Additionally, the $[Ru(bpy)_3]^{2+}$ broadened the range of

Table 4 Metal-organic framework-based photoelectrochemical detection sensors for tracing environmental pollutants^a

Working electrode	Analyte	LOD	Linear concentration range	Ref.
Eu-MOF	Fe ³⁺	0.0899 μM	1 μM~100 mM	104
Cu-MOF-NH ₂	Kanamycin	0.1 nM	0.5 nM∼650 nM	105
NiPc-Ni MOF	Curcumin	0.8 nM	2.5 nM~16 μM	106
Cu-BTC/g-C ₃ N ₄	Glyphosate	0.13 pM	1 pM∼10 nM	100
Cu-BTC@Cu₂O	Dioctyl phthalate	9.15 pM	25.0 pM~0.1 μM	107
PCN-224/rGO	<i>p</i> -arsanilic acid	5.47 ng L^{-1}	$10 \text{ ng L}^{-1} \sim 10 \text{ mg L}^{-1}$	108
CdS QDs/PCN-224	Doxorubicin hydrochloride	3.57 nM	10 nM~1 μM	102
	Gentamicin sulfate	0.158 nM	1 nM~1 μM	
PCN-222@g-C ₃ N ₄	Kanamycin sulfate	0.127 nM	1 nM∼100 nM	101
Ce-Por-MOFs/AgNWs	Ronidazole	0.038 nM	0.1 nM∼104 nM	109
$ZIF-8@ZnIn_2S_4$	Tetracycline	0.1 pM	1 pM∼700 pM	95
MIP@NH ₂ -MIL-125(Ti)/TiO ₂	Oxytetracycline	60 pM	0.1 nM~10 μM	97
CdS/Eu-MOF	Ampicillin	0.093 nM	0.1 nM~0.2 μM	110
$[Ru(bpy)_3]^{2+}$ @Ce-UiO-66/Mn:Bi ₂ S ₃	Ofloxacin	6 pM	0.01 nM~100 nM	98
g-C ₃ N ₄ /Au/NH ₂ -UiO-66	p-penicillamine	0.0046 μM	10 nM~400 μM	99
Er-MOF@AuNPs	Aflatoxin B1	$19.6 \; \mathrm{fg} \; \mathrm{mL}^{-1}$	$0.005~\text{ng mL}^{-1} \sim 10.0~\text{ng mL}^{-1}$	111

^a Eu-MOF: europium(III)-based metal organic framework; Cu-MOF-NH₂: copper(II) 2-aminoterephthalic acid; NiPc-Ni MOF: nickel phthalocyanine-based metal organic framework; Cu-BTC: copper(II) benzene-1,3,5-tricarboxylate; Ce-Por-MOFs: Ce-porphyrin-metal-organic frameworks; NH₂-MIL-125(Ti): amino-functionalized titanium(IV) based MOFs; ZIF-8: zeolitic imidazolate framework-8; CdS QDs: CdS quantum dots; PCN-222, PCN-224: zirconium-porphyrin metal-organic framework; Ce-UiO-66: Ce doped zirconium-based MOF with terephthalic acid ligands; NH₂-UiO-66: zirconium-based MOF with 2-aminoterephthalic acid ligands; Er-MOF: erbium(III)-based metal organic framework.

RSC Advances Review

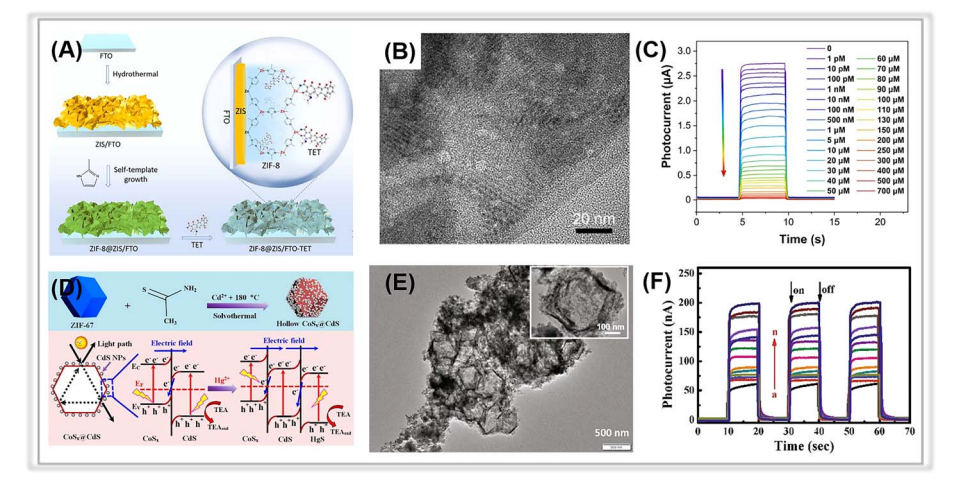


Fig. 5 (A) The preparation of a ZIF-8@ZIS-based PEC sensor for tetracycline. (B) TEM image of ZIF-8@ZIS. (C) The corresponding calibration curve for the photocurrent signal responses toward various concentrations of tetracycline. Adopted from ref. 95. Copyright 2022, with permission of Elsevier. (D) The synthetic process of hollow $CoS_x@CdS$ composites and the band structures of $CoS_x@CdS/HgS$ composites and charge separation under visible light irradiation. (E) TEM image of $CoS_x@CdS$ composites. (F) Photocurrent responses of the $CoS_x@CdS$ -modified electrodes in the presence of Hg^{2+} of different concentrations. Adopted from ref. 103. Copyright 2020, with permission of Elsevier.

light absorption, and Mn:Bi₂S₃ acted as a photosensitizer, improving the separation efficiency of photogenerated charge pair. The photocurrent response of [Ru(bpy)₃]²⁺(a)Ce-UiO-66/ Mn:Bi₂S₃ composite was improved in comparison to Mn:Bi₂S₃. Thus, the composite-modified photoelectrodes showed excellent photoelectrochemical detection activity (concentration range: 0.1~100 nM, LOD: 6 pM). Similarly, in a study by Wu and co-workers, a photoelectrochemical sensor based on Au NPs loaded on porous g-C₃N₄ nanosheets and hexagonal NH₂-UiO-66 composite (g-C₃N₄/Au/NH₂-UiO-66) was constructed for the detection of D-penicillamine.99 The presence of the Z-scheme heterojunction in g-C₃N₄/Au/NH₂-UiO-66 promoted the photogenerated electron transfer, and the strong binding between Au NPs and p-penicillamine enhanced the selectivity and sensitivity of the sensor. The composite-modified electrode exhibited a maximum photocurrent about 10 times larger than that of g-C₃N₄. Thus, the proposed g-C₃N₄/Au/NH₂-UiO-66-based photoelectrode demonstrated a low detection limit of 0.0046 µM in a wide linear range from 10 nM to 400 µM.

2.2.4. Cu-BTC. In addition to the aforementioned MIL, ZIF, and UiO series MOFs, several other MOFs, such as Cu-BTC (HKUST-1), have been employed in the fabrication of PEC sensing platforms. As for Cu-BTC, it consists of copper ions and benzene-1,3,5-tricarboxylate ligands. In 2019, Cao *et al.* constructed a PEC sensor for glyphosate assays utilizing a porous Cu-BTC/g- C_3N_4 composite. ¹⁰⁰ Porous Cu-BTC offered the benefit of trapping glyphosate molecules and significantly enhanced the photoelectric conversion efficiency of g- C_3N_4 nanosheets. In this detection system, the formation of the Cu-glyphosate complex increased the steric hindrance to electron transfer between the composite and the electrode surface, leading to a reduction of photocurrent. Thus, a correlation between photocurrent and glyphosate concentration was established over a wide range from 1 pM to 1 nM.

2.2.5. PCN. PCN is a type of MOF comprising zirconium (Zr) clusters and porphyrin ligands. Its remarkable stability and photoelectrochemical properties make it highly promising for the fabrication of PEC platforms. For instance, Dong and coworkers constructed a photoelectrochemical sensor for the identification of kanamycin sulfate based on a PCN-222@g-C₃N₄ composite. 101 Through a physical microwave mixing process, g-C₃N₄ with a broad bandgap was effectively coupled with porous, narrow-band gap PCN-222. The compositemodified photoelectrode demonstrated a low detection limit of 0.127 nM with a wide linear range from 1 nM to 1000 nM. Similar work has also been conducted employing the CdS QDs/ PCN-224 composite.102 Sub-3 nm CdS quantum dots were uniformly distributed in the porous PCN-224. Compared to pure PCN-224 and CdS QDs, the photocurrent response of the composite-based electrode was improved. With regard to the detection of doxorubicin hydrochloride and gentamicin sulfate, the LODs were as low as 3.57 nM and 0.158 nM, respectively.

2.2.6. Ln-MOFs. Some other Ln-MOFs have also been employed in the fabrication of PEC sensing platforms. Eu-MOFs, as a representative class of Ln-MOFs, possess excellent light-harvesting properties. For instance, Gao *et al.* prepared a CdS nanoparticle/europium metal–organic framework (CdS/Eu-MOF) composite and utilized it for PEC monitoring of ampicillin. The porous structure of the Eu-MOF enhanced the light absorption capability of the composite while effectively inhibiting the recombination of photogenerated charge pairs. The CdS/Eu-MOF-based PEC sensor achieved a low detection limit of around 0.093 nM, along with great selectivity, outstanding repeatability, and desired stability. In summary, porous metal–organic frameworks have demonstrated remarkable potential for photoelectrochemical sensing of environmental toxic species.

2.2.7. MOF derivatives. Moreover, MOF derivatives have shown potential for identifying toxic species in the environment^{116,120,123} (Table 5). For instance, Zhang *et al.* prepared

Review **RSC Advances**

hollow CoS_x@CdS polyhedron composite for photoelectrochemical Hg²⁺ assays. The composites were obtained by decorating CdS nanoparticles on the surface of CoSx through a simple solvothermal method, using a zeolitic imidazolate framework-67 (ZIF-67) as the sacrificial template and cobalt precursor¹⁰³ (Fig. 5D). The porous CoS_r polyhedron component in the composite facilitates the transfer of photogenerated electrons during the PEC detection process (Fig. 5E). The photocurrent of the CdS/CoS_r composite-modified electrode was about 50 nA, 2.5 times higher than that of CdS. Photoluminescence spectra (PL) and electrochemical impedance spectroscopy (EIS) measurements also confirmed its enhanced photogenerated charge pair separation ability. Compared to the CdS or CoS_x modified electrodes, the CdS/CoS_x modified electrode exhibited an increasing photocurrent in the presence of analyte-Hg²⁺ due to the *in situ* formation of a Z-scheme CoSx@CdS/HgS via a selective ionexchange reaction. A strong linear relationship was established between the photocurrent and log(Hg²⁺) concentrations in the range of 0.005 nM to 1000 nM, with a LOD of 0.002 nM (Fig. 5F).

Derivatives of the MIL family of MOFs have also demonstrated excellent PEC detection activities against environmental toxic species. In a study by Zhang and co-workers, COOHfunctionalized TiO2 (TiO2-C) was achieved via one-step calcination of MIL-125(Ti).114 Due to the large specific surface area and abundant functional groups of TiO2-C, it demonstrated superior photochemical, electrochemical, and PEC detection performance compared to MIL-125(Ti). Furthermore, it was also useful for grafting molecularly imprinted polymers (MIPs). The MIPs@TiO2-C, with a large number of binding sites, provides precise electron transfer channels, resulting in improved sensitivity and selectivity for antibiotics such as ofloxacin. Under optimal conditions, the prepared sensor has a low detection limit (2.9 pg mL⁻¹) and a wide linear concentration range (0.01 ng mL $^{-1}$ \sim 3 µg mL $^{-1}$).

MIL-68(In) is also an ideal template for obtaining porous photoactive materials. For instance, Yan et al. synthesized an In₂O₃-In₂S₃-Ti₃C₂ MXene composite on the base of MIL-68(In)derived In2O3 hollow tubular122 and then used it to construct a dual-mode (photoelectrochemical and photofuel cell) self-

powered apta-sensing platform for detecting microcystin-LR (MC-LR). Porous In₂O₃ hollow tubulars with a large specific surface area provide abundant active sites, while the wellmatched energy levels of In2O3 and In2S3 and the Ti3C2 MXene quantum dots acting as electron transfer mediators both accelerate the separation of photogenerated charge carriers. This sensing platform revealed excellent PEC detection activity in the range from 0.5 pM to 400 nM, with a LOD of 0.169 pM. In another research, Feng et al. used MIL-68(In) as the precursor for fabricating homogeneous In2O3 nanoparticles through high temperature calcination in an air atmosphere. 120 The formation of a heterojunction between the porous In₂O₃ and g-C₃N₄ facilitated the separation and transfer of photogenerated charge pairs. The introduction of gold nanoparticles (Au NPs) with the localized surface plasmon resonance (LSPR) effect also improved visible light absorption and photoelectron transfer. The photocurrent of the Au NPs/In₂O₃(@g-C₃N₄ composite reached 1.75 µA, much larger than that of pure g-C₃N₄. The Au NPs/In₂O₃@g-C₃N₄ was successfully applied to fabricate a label-free photoelectrochemical apta-sensing platform for tetracycline detection, which yielded a wide linear range from 0.01 nM to 500 nM with a LOD of 3.3 pM. Porous composites derived from Cu-BTC or Zn-BTC have also demonstrated great potential for PEC detection. In a study by Cao et al., Cu-BTC MOF (BTC: benzene-1,3,5-tricarboxylic acid) was calcinated to achieve porous hierarchical CuO. 115 The CuO material has a large specific surface area, which is favorable for the capture of the target species, malathion. The facile PEC detection sensor achieved a LOD of 0.086 nM in the range of 0.1 nM to 104 nM.

2.3. Covalent organic frameworks

Like metal-organic frameworks, covalent organic frameworks (COFs) are a new class of porous materials that have attracted much interest for constructing the PEC analytic platforms. 128,129 Generally, COFs are composed of covalently bonded light elements, such as C, N, H, O, B, and Si. The porous nature of COFs favors the trapping of probe species such as heavy metal

Table 5 Derivatives of metal-organic framework based photoelectrochemical detection sensors for environmental pollutant assay^a

Working electrode	Template MOF	Analyte	LOD	Linear concentration range	Ref.
CoS _x @CdS	ZIF-67	Hg^{2^+}	0.002 nM	0.01 nM~1 μM	103
Cu ₂ O/CuO/TiO ₂	NH ₂ -MIL-125(Ti)	Pb^{2+}	6.8 fM	10 fM \sim 1 μ M	112
$CdCoS_2$	ZIF-67-S	Chlorpyrifos	0.57 ng mL^{-1}	$0.001 \ \mu g \ mL^{-1} \sim 270 \ \mu g \ mL^{-1}$	113
MIPs@TiO ₂ -C	MIL-125(Ti)	Ofloxacin	2.91 pg mL^{-1}	$0.01 \text{ ng mL}^{-1} \sim 3 \mu\text{g mL}^{-1}$	114
CuO	Cu-BTC	Malathion	0.086 nM	0.1 nM∼104 nM	115
ZnO-Co ₃ O ₄	Zn-BTC	Sulfadiazine	1.2 nM	$0.005~\mu M{\sim}18.5~\mu M$	116
ZnO/g-C ₃ N ₄	ZIF-8	Oxytetracycline	1.49 fM	5 fM∼200 nM	117
$ZnIn_2S_4$ @ TiO_2	ZIF-8	Lincomycin	0.084 pM	0.1 pM∼0.1 nM	118
$ZnCdS@MoS_2$	ZIF-8	Lincomycin	0.076 nM	0.1 nM∼300 nM	119
AuNPs/In ₂ O ₃ @g-C ₃ N ₄	MIL-68(In)	Tetracycline	3.3 pM	0.01 nM~0.5 μM	120
$Zn_xCo_{3-x}O_4/N$ -GQDs/AgBiS ₂	ZnCo-ZIF	Ampicillin	0.25 pM	0.5 pM∼10 nM	121
In ₂ O ₃ -In ₂ S ₃ -Ti ₃ C ₂ MXene	MIL-68(In)	Microcystin-LR	0.169 pM	0.5 pM~400 nM	122

^a ZIF-67: zeolitic imidazolate framework-67; MIPs: molecularly imprinted polymers; ZIF-8: zeolitic imidazolate framework-8; MIL-125(Ti): titanium(w) terephthalic acid; Cu-BTC: Cu-BTC: copper(u) benzene-1,3,5-tricarboxylate; Zn-BTC: Zn(u) benzene-1,3,5-tricarboxylate; MIL-68(In): In(III) 1,4-benzenedicarboxylate; ZnCo-ZIF: bimetallic ZnCo-zeolitic imidazolate framework.

RSC Advances Review

ions. Moreover, the electronic interactions between the COF layers are realized by the π -stacked aromatic subunits, providing sufficient channels for charge transport. 30-132 So far, several COFs have been employed in the field of PEC detection, such as D-TA COF, 133,134 TAPP-COF, 124 TTPA-COF, 135 F-COF, 125 pbqy-COF,136 and PFA-130.137 However, the studies on PEC sensors based on covalent organic frameworks for tracing environmental pollutants are still in their early stages, as summarized in Table 6. In a study by Zhao and co-workers, a porphyrin-based covalent organic framework thin film (TAPP-COF) was synthesized via a liquid-liquid interfacial method and used as a photocathode material for photoelectrochemical "on-off-on" sensing of Pb2+.124 Due to the unique charge channels of porous COFs and the excellent photoelectric properties of porphyrin, 138 the TAPP-COF-based PEC sensor displayed an improved "signal-on" photocathodic current response. The CdSe@SiO2 quantum dots, as a quenching agent, were introduced via a hybridization chain reaction to achieve a "signal off" photocurrent response, and then the PEC response switched to a "signal on" state after the addition of the detected species, Pb2+ (Fig. 6A). TAPP-COF is a p-type material that is beneficial to photogenerated electron-hole pair transfer. ¹³⁹ Hence, the as-prepared PEC detection sensor displayed a wide linear range from 0.05 nM to 100 nM with a LOD of 0.012 nM (Fig. 6C). Moreover, the flexibility of TAPP-COFs film was excellent, indicating its broad potential application in wearable PEC sensing devices (Fig. 6B). ¹⁴⁰⁻¹⁴⁵

Alternatively, the combination of COFs with other materials could enhance their performance in PEC detection platforms by providing more reactive sites for the determination of target environmental contaminants. In a study by Wang et al., a heterostructure was formed between TiO2 NTAs and F-COFs through a simple hydrothermal method (Fig. 6D and E) and then used for constructing a PEC detection platform for dopamine.125 The introduction of F-COFs enhanced the visible light absorption and photogenerated electron-hole pairs separation efficiency. Meanwhile, the porous F-COFs processed a large specific surface area, and π - π interactions could be formed between aromatics of dopamine,146 which contributed to their ultra-sensitive detection activity. The resulting PEC sensor demonstrated excellent photocurrent response stability. More importantly, a LOD of 0.032 µM was obtained in an extended linear range (Fig. 6F).

Table 6 Covalent organic framework-based photoelectrochemical monitoring of environmental pollutants^a

Working electrode	Analyte	LOD	Linear concentration range	Ref.
TAPP-COF	Hg ²⁺	0.012 nM	0.05 nM∼1000 nM	124
CoPc-PT-COF@Cu-MOF	Cr(III)	14.5 fM	0.1 pM∼100 nM	126
F-COF/TiO ₂ NTAs	Dopamine	0.032 μΜ	0.1 μM~300 μM	125
NH ₂ -UiO-66/TpPa-1-COF	Dibutyl phthalate	30 pM	0.1 nM~100 μM	127

^a TAPP-COF: porphyrin-based covalent organic framework; CoPc-PT-COF: tetra-amine cobalt phthalocyanine-2,9-bis[p-(formyl) phenyl]-1,10-phenanthroline-covalent organic framework; F-COF: fluoro-substituted covalent organic frameworks; TpPa-1-COF: p-phenylenediamine-covalent organic framework.

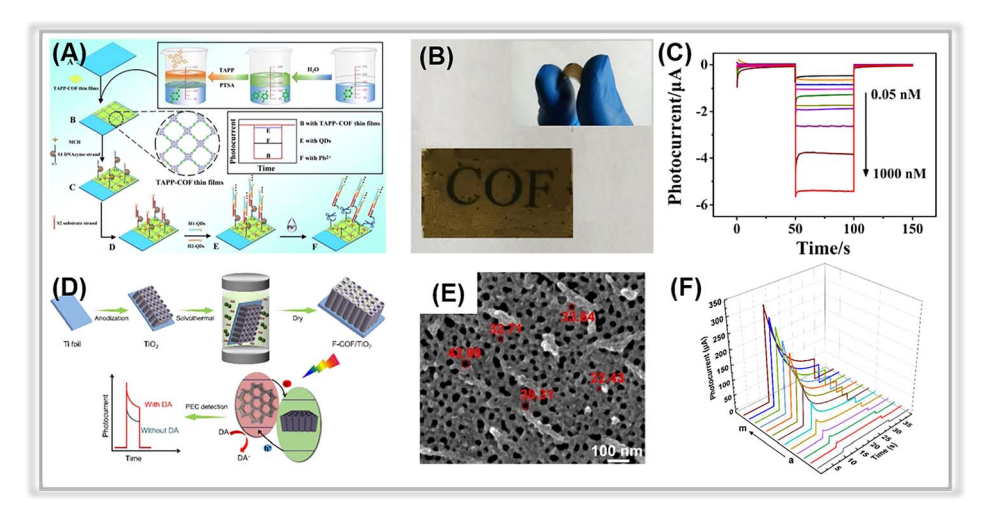


Fig. 6 (A) Illustration of the TAPP-COF-based PEC sensor for tracing Pb^{2+} . (B) The flexible photograph of TAPP-COF thin films. (C) Photocurrent response of the photoelectrochemical detection sensor to different concentrations of Pb^{2+} . Adopted from ref. 124. Copyright 2021, with permission of American Chemical Society. (D) The construction of the F-COF/TiO₂ NTA platform for PEC sensing for dopamine. (E) SEM image of F-COF/TiO₂ NTA. (F) Photocurrent response of F-COF/TiO₂ NTA to different concentrations of dopamine. Adopted from ref. 125. Copyright 2021, with permission of American Chemical Society.

Review Heterostructure COF/MOF hybrids have been fabricated as 2.4. Graphitic carbon nitride

multifunctional materials for sensing applications. 127,147 In 2021, Zhang et al. prepared a CoPc-PT-COF@Cu-MOF-based PEC-EC dual-mode biosensor for Cr(III) quantification. 126 The 2D CoPc-PT-COF was in situ grown on a Cu-MOF by covalent binding between the carboxyl group in the Cu-MOF and the amino group in the CoPc-PT-COF. The DNA strands could be easily anchored on the composite via strong interaction owing to its large specific surface area and high porosity. Furthermore, due to the specific recognition between DNA and Cr(III), the composite-based biosensor could be used to trace Cr(III). The photocurrent of composite (419 nA) was about 14.5 times greater than that of Cu-MOF, indicating that the heterojunction between Cu-MOF and CoPc-PT-COF enhanced the photoelectric conversion efficiency. So, the obtained composite-based PEC biosensor displayed a LOD of 14.5 fM within the Cr(III) concentration range of 0.1 pM to 100 nM. Overall, porous COFs have significant potential for PEC sensing applications against environmental contaminants.

Graphitic carbon nitride (g-C₃N₄) is a well-known metal-free polymeric semiconductor that exhibits excellent visible light response and environmental friendliness. 148-151 In recent years, g-C₃N₄ has been utilized in the area of PEC detection of environmental contaminants120,152-156 (Table 7). However, for bulk g- C_3N_4 , the PEC detection performance is poor due to its relatively low photoelectric conversion efficiency. Activating pristine g-C₃N₄ with various treatments to achieve a porous structure is indeed an excellent way to speed up the separation of photogenerated charge pairs. Specifically, the methods employed to treat bulk g-C3N4 include chemical exfoliation and thermal oxidation.149,157,158

For the chemical exfoliation process, the morphology and porosity of the porous carbon nitride are determined by the choice of etchant and the reaction conditions. 159 Common exfoliation agents include K₂Cr₂O₇ + H₂SO₄, KMnO₄ + H₂SO₄, and HNO₃ + H₂SO₄.¹⁶⁰ However, these chemical agents pose environmental and safety concerns due to their hazardous nature. Thermal oxidation is another method for producing

Table 7 Graphitic carbon nitride-based PEC sensing platform for tracing environmental pollutants^a

$ \begin{array}{c ccccccccccccccccccccccccccccccccccc$	163 43 164 165 166 167 168
$\begin{array}{cccccccccccccccccccccccccccccccccccc$	164 165 166 167
$ \begin{array}{cccccccccccccccccccccccccccccccccccc$	165 166 167
$\begin{array}{cccccccccccccccccccccccccccccccccccc$	166 167
$\begin{array}{cccccccccccccccccccccccccccccccccccc$	167
$\begin{array}{cccccccccccccccccccccccccccccccccccc$	
$\begin{array}{cccccccccccccccccccccccccccccccccccc$	168
Hg²+ 0.22 nM 0~500 nM ND-g-CN Ciprofloxacin 20 ng L⁻¹ 60 ng L⁻¹~19.1 μg L⁻¹ CNNS-Cu p-Nitrotoluene 0.13 μΜ 0.1 μΜ~100 μΜ Au/PCN-S Oxytetracycline 0.34 nM 0.5 nM~200 nM Bi/BiVO ₄ /g-C₃N₄ Oxytetracycline 0.0033 nM 0.01 nM~1000 nM Bi/CV-PCN Enrofloxacin 3.3 fg mL⁻¹ 0.01 pg mL⁻¹~1 μg mL⁻¹ Au-doped 3D CN Chloramphenicol 0.1 pM 0.5 pM~300 nM α-Fe₂O₃/d-C₃N₄ Penbritin 0.0125 pM 0.5 pM~50 nM ZnPc/CN Sulfadimethoxine 0.03 nM 0.1 nM~300 nM BiFeO₃/utg-C₃N₄ Ampicillin 0.33 pM 1 pM~1 μM ZnIn₂S₄/g-C₃N₄ Bisphenol A 0.016 μΜ 0.05 μM~30 μM g-C₃N₄/BiOI Bisphenol A 26 ng mL⁻¹ 80 ng mL⁻¹~3.2 μg mL⁻¹	
ND-g-CN Ciprofloxacin 20 ng L ⁻¹ 60 ng L ⁻¹ ~19.1 μg L ⁻¹ CNNS-Cu p -Nitrotoluene 0.13 μM 0.1 μM~100 μM Au/PCN-S Oxytetracycline 0.34 nM 0.5 nM~200 nM Bi/BiVO ₄ /g-C ₃ N ₄ Oxytetracycline 0.0033 nM 0.01 nM~1000 nM Bi/CV-PCN Enrofloxacin 3.3 fg mL ⁻¹ 0.01 pg mL ⁻¹ ~1 μg mL ⁻¹ Au-doped 3D CN Chloramphenicol 0.1 pM 0.5 pM~300 nM α-Fe ₂ O ₃ /d-C ₃ N ₄ Penbritin 0.0125 pM 0.5 pM~50 nM ZnPc/CN Sulfadimethoxine 0.03 nM 0.1 nM~300 nM BiFeO ₃ /utg-C ₃ N ₄ Ampicillin 0.33 pM 1 pM~1 μM ZnIn ₂ S ₄ /g-C ₃ N ₄ Bisphenol A 0.016 μM 0.05 μM~30 μM g-C ₃ N ₄ /BiOI Bisphenol A 26 ng mL ⁻¹ 80 ng mL ⁻¹ ~3.2 μg mL ⁻¹	
CNNS-Cu p -Nitrotoluene 0.13 μ M 0.1 μ M \sim 100 μ M Au/PCN-S Oxytetracycline 0.34 nM 0.5 nM \sim 200 nM Bi/Bi/VO ₄ /g-C ₃ N ₄ Oxytetracycline 0.0033 nM 0.01 nM \sim 1000 nM Bi/CV-PCN Enrofloxacin 3.3 fg mL $^{-1}$ 0.01 pg mL $^{-1}$ \sim 1 μ g mL $^{-1}$ Au-doped 3D CN Chloramphenicol 0.1 pM 0.5 pM \sim 300 nM α -Fe ₂ O ₃ /d-C ₃ N ₄ Penbritin 0.0125 pM 0.5 pM \sim 50 nM ZnPc/CN Sulfadimethoxine 0.03 nM 0.1 nM \sim 300 nM BiFeO ₃ /utg-C ₃ N ₄ Ampicillin 0.33 pM 1 pM \sim 1 μ M ZnIn ₂ S ₄ /g-C ₃ N ₄ Bisphenol A 0.016 μ M 0.05 μ M \sim 30 μ M g-C ₃ N ₄ /BiOI Bisphenol A 26 ng mL $^{-1}$	
Au/PCN-S Oxytetracycline 0.34 nM 0.5 nM \sim 200 nM Bi/BiVO ₄ /g-C ₃ N ₄ Oxytetracycline 0.0033 nM 0.01 nM \sim 1000 nM Bi/CV-PCN Enrofloxacin 3.3 fg mL $^{-1}$ 0.01 pg mL $^{-1}$ \sim 1 μg mL $^{-1}$ Au-doped 3D CN Chloramphenicol 0.1 pM 0.5 pM \sim 300 nM α-Fe ₂ O ₃ /d-C ₃ N ₄ Penbritin 0.0125 pM 0.5 pM \sim 50 nM ZnPc/CN Sulfadimethoxine 0.03 nM 0.1 nM \sim 300 nM BiFeO ₃ /utg-C ₃ N ₄ Ampicillin 0.33 pM 1 pM \sim 1 μM ZnIn ₂ S ₄ /g-C ₃ N ₄ Bisphenol A 0.016 μM 0.05 μM \sim 30 μM g-C ₃ N ₄ /BiOI Bisphenol A 26 ng mL $^{-1}$ 80 ng mL $^{-1}$ \sim 3.2 μg mL $^{-1}$	169
$\begin{array}{cccccccccccccccccccccccccccccccccccc$	170
Bi/CV-PCN Enrofloxacin 3.3 fg mL^{-1} $0.01 \text{ pg mL}^{-1} \sim 1 \text{ μg mL}^{-1}$ Au-doped 3D CN Chloramphenicol 0.1 pM $0.5 \text{ pM} \sim 300 \text{ nM}$ α-Fe ₂ O ₃ /d-C ₃ N ₄ Penbritin 0.0125 pM $0.5 \text{ pM} \sim 50 \text{ nM}$ ZnPc/CN Sulfadimethoxine 0.03 nM $0.1 \text{ nM} \sim 300 \text{ nM}$ BiFeO ₃ /utg-C ₃ N ₄ Ampicillin 0.33 pM $1 \text{ pM} \sim 1 \text{ μM}$ ZnIn ₂ S ₄ /g-C ₃ N ₄ Bisphenol A 0.016 μM $0.05 \text{ μM} \sim 30 \text{ μM}$ g-C ₃ N ₄ /BiOI Bisphenol A 26 ng mL^{-1} $80 \text{ ng mL}^{-1} \sim 3.2 \text{ μg mL}^{-1}$	162
Au-doped 3D CN Chloramphenicol 0.1 pM 0.5 pM \sim 300 nM α-Fe ₂ O ₃ /d-C ₃ N ₄ Penbritin 0.0125 pM 0.5 pM \sim 50 nM ZnPc/CN Sulfadimethoxine 0.03 nM 0.1 nM \sim 300 nM BiFeO ₃ /utg-C ₃ N ₄ Ampicillin 0.33 pM 1 pM \sim 1 μM ZnIn ₂ S ₄ /g-C ₃ N ₄ Bisphenol A 0.016 μM 0.05 μM \sim 30 μM g-C ₃ N ₄ /BiOI Bisphenol A 26 ng mL ⁻¹ 80 ng mL ⁻¹ \sim 3.2 μg mL ⁻¹	171
$ \begin{array}{cccccccccccccccccccccccccccccccccccc$	172
$ \begin{array}{cccccccccccccccccccccccccccccccccccc$	173
$\begin{array}{cccccccccccccccccccccccccccccccccccc$	62
ZnIn ₂ S ₄ /g-C ₃ N ₄ Bisphenol A 0.016 μM 0.05 μM \sim 30 μM g-C ₃ N ₄ /BiOI Bisphenol A 26 ng mL ⁻¹ 80 ng mL ⁻¹ \sim 3.2 μg mL ⁻¹	174
g-C ₃ N ₄ /BiOI Bisphenol A 26 ng mL ⁻¹ 80 ng mL ⁻¹ \sim 3.2 μ g mL ⁻¹	175
	156
	176
g-C ₃ N ₄ /CuO Bisphenol A 6.2 ng L ⁻¹ 0.02 ng L ⁻¹ \sim 10 ng L ⁻¹	177
NiO-Ni-GCN Octylphenol 3.3 nM $10 \text{ nM} \sim 1 \mu\text{M}$	178
$g-C_3N_4/Bi_{24}O_{31}Cl_{10}$ Enrofloxacin 0.167 fM 0.5 fM \sim 100 fM	179
Bi/CV-PCN Enrofloxacin 3.3 fg mL $^{-1}$ 0.01 pg mL $^{-1}$ \sim 1 μ g mL $^{-1}$	172
S-BN/Au/CN Diazinon 6.8 pM 0.01 nM~100 nM	180
CoN/g-C ₃ N ₄ Atrazine $3.3 \times 10^{-5} \text{ fM}$ $1.0 \times 10^{-4} \text{ fM} \sim 10 \text{ fM}$	181
Ag_2CrO_4/g - C_3N_4/GO Chloramphenicol 0.29 pM 0.5 pM \sim 50 nM	182
g- C_3N_4 -AuNPs Triclosan 0.601 pM 2 pM \sim 800 pM	183
C_3N_4 -rGO Rutin 1.78 nM 5 nM \sim 140 μ M	184
$\label{eq:coomer} {\sc CoO/Au/g-C_3N_4} \qquad \qquad {\sc Microcystin-LR} \qquad \qquad 0.01 \ pM \qquad \qquad 0.1 \ pM{\sim}10 \ nM$	185
BiVO ₄ /2D-C ₃ N ₄ Microcystin-LR 0.042 pg L ⁻¹ 0.5 pg L ⁻¹ \sim 10 μ g L ⁻¹	186

^a A-CN: alkalized C₃N₄; 3DBC-C₃N₄: three-dimension branched crystalline carbon nitride; GA-C₃N₄: graphene-analogue carbon nitride; F-g-C₃N₄: formate anion-incorporated graphitic carbon nitride; Au/PCN-S: Au nanoparticle-decorated phosphorus-doped porous ultrathin C3N4 nanosheets; Au-doped 3D CN: Au nanoparticle doped three-dimensional graphitic carbon nitride; CNNS-Cu: copper cluster modified carbon nitride nanosheets; ZnPc/CN: zinc phthalocyanine/graphitic carbon nitride; utg-C₃N₄: ultrathin graphite-like carbon nitride; S-BN/Au/CN: sulfur doped hexagonal boron nitride/Au nanoparticles/graphitic carbon nitride; CB: carbon black; NS: nanosheets.

RSC Advances Review

porous carbon nitride. This process disrupts the hydrogen bonds in carbon nitride framework, leading to the formation of porous carbon nitride nanosheets with a large specific surface area and a thin sheet structure.161 However, those above two aforementioned approaches can harm the environment. Further, it requires high-quality bulk g-C₃N₄, and the process is complicated and time-consuming.

For instance, in a study by Peng and co-workers, phosphorus-doped porous carbon nitride nanosheets (PCN-S) were synthesized using element doping and thermal oxidation method.162 The PCN-S demonstrated an ultrathin nanosheet structure, a large specific surface area, and numerous surface pores (Fig. 7D). Moreover, the Au NPs with the LSPR effect were in situ decorated on the porous surface to yield an Au/PCN-S composite via a photo-reduction method. The composite was used to construct a self-powered PEC apta-sensor for the oxytetracycline (OTC) assay. Under visible light irradiation, electrons were excited to the CB of PCN-S and subsequently transferred to the Au NPs. They then reacted with dissolvable oxygen in the aqueous solution to produce superoxide oxygen species, which react with analyte-OTC (Fig. 7F). Owing to its strong visible light absorption ability and enhanced photogenerated charge pair separation efficiency, the Au/PCN-S composite-based PEC sensor demonstrated excellent performance in terms of a wide linear detection range ($0.5\sim200 \text{ nM}$), a low detection limit (0.34 nM) (Fig. 7E).

Different from traditional methods, alkaline hydrothermal treatment is a new effective approach to achieving porous carbon nitride nanosheets. 187,188 In 2020, Liang et al. prepared a porous carbon nitride via an alkaline hydrothermal method. 163 The hydroxide effectively exfoliated the 2D framework of the pristine bulk graphitic carbon nitride to obtain a porous structure with a large number of functional groups on its surface. The TEM image of activated g-C₃N₄ (A-CN) clearly revealed the presence of porous structures on its surface

(Fig. 7A). Moreover, the specific surface area (SSA) of A-CN was about 10 times larger than that of bulk g-C₃N₄ (Fig. 7B), further confirming the existence of porous structures in A-CN. In Fig. 7C, the photocurrent response of A-CN was much higher than that of bulk g-C₃N₄ due to the porous structure and the large number of functional groups on the surface, which promoted photogenerated charge separation and transfer. Thus, the A-CN-based PEC sensor displayed an outstanding performance for Cu²⁺ detection with a low detection limit of $0.31 \mu M$ in the range from $0.2 \mu M$ to $50 \mu M$.

Aiming to overcome the inevitable restacking and agglomeration of the bulk g-C₃N₄ nanosheets, the fabrication of threedimensional (3D) porous g-C₃N₄ is another simple method. It not only prevents the agglomeration of nanosheets but also improves the utilization of irradiation through multiple reflections in its open framework. 189,190 For instance, Zhang et al. developed a dual-photoelectrode for detecting chloramphenicol, employing Au NPs doping porous three-dimensional g-C₃N₄ and porous N-doped Cu₂O/C used as the photoanode and photocathode, respectively.¹⁷³ The small-scale Au NPs were uniformly distributed across the 3D CN nanosheets. The photocurrent of Au-doped 3D CN was much higher than that of bulk g-C₃N₄, and it also had the smallest electron transfer resistance. The porous 3D g-C₃N₄ improved both the visible light absorption ability and photoelectric conversion efficiency. Additionally, the presence of Au NPs with the LSPR effect provided extra energy for photogenerated charge carrier generation with the aid of hot electron transfer. As a result, the prepared apta-sensor exhibited an ultra-low detection limit (0.1 pM) and a wide linear detection range (0.5 pM \sim 300 nM).

2.5. MXene

MXene, a 2D transition metal carbide or nitride, has been widely used in various applications, including electromagnetic shielding, interference energy storage batteries,

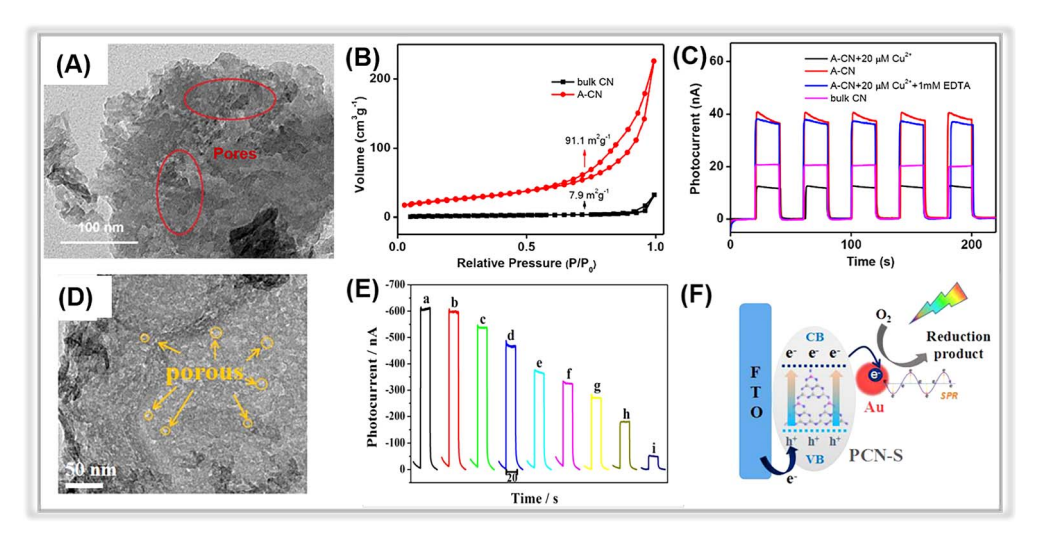


Fig. 7 (A) TEM image of A-CN. (B) Nitrogen adsorption—desorption isotherm curves for bulk CN and A-CN. (C) Photocurrent responses of bulk CN and A-CN. Adopted from ref. 163. Copyright 2020, with permission of Elsevier. (D) TEM images of PCN-S. (E) Photocurrent responses of the Au/PCN-S at various oxytetracycline concentrations. (F) The photocurrent generation mechanism of Au/PCN-S under visible light irradiation. Adopted from ref. 162. Copyright 2018, with permission of Elsevier.

supercapacitors, and sensors.^{38,191–194} Porous MXenes have demonstrated outstanding chemical reactivity and hydrophilicity owing to their superior electrical conductivity and significant number of functional groups like –F and –OH, enabling them to form heterojunctions with semiconductors.¹⁹⁵ Additionally, exposed connector metal sites, such as titanium on MXenes, present a higher redox reactivity compared to conventional carbon materials, positioning MXene nanolayers as ideal optoelectronic platforms. Recent reports on MXenebased PEC sensors for environmental pollutant detection are summarized in Table 8. These reports illustrate that MXene can be combined with a variety of materials, including graphene oxide, graphitic carbon nitride, metal oxide, metal halide, and metal sulfide, to construct composite hybrid photo-

electrochemical detection platforms.

Graphene oxide and graphitic carbon nitride can be effectively coupled with the porous MXenes due to the strong π - π interaction between them. 196,197 For instance, in a study by Yuan and co-workers, the g-C₃N₄/Ti₃C₂ MXene composite was synthesized and proposed as a PEC sensing material for ciprofloxacin detection.196 In Fig. 8A, porous Ti₃C₂ MXene was observed on the surface of g-C₃N₄, suggesting a close connection between the two components facilitated by electrostatic self-assembly. Transient photocurrent measurements (Fig. 8B) revealed a photocurrent density of 1.36 μA cm⁻² for the g-C₃N₄/ Ti₃C₂ MXene, nearly twice that of g-C₃N₄. Meanwhile, the EIS of g-C₃N₄/Ti₃C₂ MXene has a smaller arc size compared to that of pure g-C₃N₄. These findings suggested that the introduction of Ti₃C₂ MXene promotes photogenerated charge transfer. The fabricated PEC sensor demonstrated an ultra-low detection limit of 0.13 nM over a broad linear range from 0.4 nM to 1000 nM.

These results imply that the tight interaction between Ti_3C_2 MXene and g- C_3N_4 facilitates the smooth transfer of photogenerated electrons from g- C_3N_4 to Ti_3C_2 MXene, whose Fermi level (0.58 V νs . NHE) is much more positive than the conduction band energy of g- C_3N_4 (Fig. 8C).

Similarly, another typical carbon material, graphene oxide, has also been coupled with porous Ti₃C₂ MXene to construct smart PEC sensing platforms. In 2023, Zhang et al. reported a "signal-on" PEC sensor for sulfide detection based on in situ growth of AgI on a 3D porous Ti₃C₂ MXene/graphene aerogel (AgI/ Ti₃C₂ MXene/GO). 198 The porous Ti₃C₂ MXene/GO was synthesized through the solvothermal method, followed by in situ decoration of AgI NPs onto the Ti₃C₂ MXene/GO. Fig. 8D depicts the typical three-dimensional interconnected skeleton structure of aerogel. The porous structure of Ti₃C₂ MXene/GO aerogel with large specific surface area favored the anchoring of AgI NPs. Upon the addition of detection analyte-sulfide (S²⁻), Ag₂S formed on the surface of AgI/Ti₃C₂ MXene/GO, resulting in an enhanced photocurrent response due to the newly created Ag₂S/AgI heterojunction (Fig. 8F). As a result, the associated PEC sensor revealed an outstanding S²⁻ detection activity, including a wide linear range (5 nM \sim 200 μ M) and an ultra-low detection limit (1.54 nM).

Interestingly, MXene can serve as a co-catalyst to enhance the separation efficiency of photogenerated electron-hole pair. 204,205,212,213 Recently, porous MXenes have been combined with various semiconductors (e.g., TiO2, BiVO4, MoS2, and BiOI) to fabricate composite-based PEC platforms for environmental contaminant assays. For example, Ling and co-workers reported a PEC sensing platform based on a BiVO₄/Ti₃C₂ MXene composite for oxytetracycline (OTC) detection.205 Within the composite, the small porous MXene nanosheets acted as a cocatalyst to promote photo-generated charge pair separation. This was confirmed by the enhanced photocurrent responses, weaker PL intensity, and smaller arc resistance values of BiVO₄/ Ti₃C₂ MXene. The introduction of MXene created a Schottky barrier between BiVO₄ and MXene, effectively suppressing electron reflux. During the PEC detection process, photogenerated electrons in the CB of BiVO₄ were transferred to MXene via the Schottky junction and then injected into a conductive substrate (in this case, ITO) to generate photocurrent. Simultaneously, holes in the VB of BiVO₄ contributed to the current generation by oxidizing OTC molecules on the

Table 8 MXene-based PEC sensors for environmental pollutant detection^a

Working electrode	Analyte	LOD	Linear concentration range	Ref.
Ti ₃ C ₂ MXene/SnS ₂	Cr(vi)	0.51 pM	1.0 pM∼0.1 mM	199
Ti ₃ C ₂ MXene/BiVO ₄	Hg^{2+}	1 pM	1 pM∼2 nM	200
CdS/Ti ₃ C ₂ MXene	Cu^{2+}	0.05 nM	0.1 nM~10 μM	201
BiOBi _x I _{1-x} /Ti ₃ C ₂ MXene	Hg^{2^+}	42.1 pM	0.1 nM∼1000 nM	202
BiOI/Ti ₃ C ₂ MXene	L-cysteine	0.005 nM	0.01 nM~10 μM	203
TiO ₂₍₀₀₁₎ /Ti ₃ C ₂ MXene	Dopamine	0.52 μΜ	1.0 μM~1000 μM	204
BiVO ₄ /Ti ₃ C ₂ MXene	Oxytetracycline	0.03 nM	0.1 nM~100 nM	205
g-C ₃ N ₄ /Ti ₃ C ₂ MXene	Ciprofloxacin	0.13 nM	0.4 nM∼1000 nM	196
Ti ₃ C ₂ MXene/Bi ₄ VO ₈ Br/TiO ₂	Ciprofloxacin	0.3 nM	1 nM∼1500 nM	206
AgBr/Ti ₃ C ₂ MXene	Chlorpyrifos	$0.33 \ \mathrm{pg} \ \mathrm{L}^{-1}$	$0.001~{ m pg}~{ m L}^{-1}{\sim}1~{ m ng}~{ m L}^{-1}$	207
Bi ₄ VO ₈ Br/Ti ₃ C ₂ MXene	Streptomycin	0.3 nM	1 nM∼1000 nM	208
Au@PtAg/TiO ₂ -Ti ₃ C ₂ MXene	Ochratoxin A	1.73 fg mL^{-1}	$5 \text{ fg mL}^{-1} \sim 10 \text{ ng mL}^{-1}$	209
Anode: TiO ₂ /S-Ti ₃ C ₂ MXene	Microcystin-RR	0.034 fM	0.1 fM∼1 nM	210
Cathode: MoS ₂ /S-Ti ₃ C ₂ MXene	Aflatoxin B1	0.73 pg mL^{-1}	$0.01 \text{ pg mL}^{-1} \sim 1 \mu\text{g mL}^{-1}$	211
MoS_2 - $Ti_3C_2T_x$ MXene		- 2		
AgI/Ti ₃ C ₂ MXene/GO	Sulfide	1.54 nM	5 nM~200 μM	198

^a TiO₂₍₀₀₁₎; active surface (001 facet) TiO₂; AgI/Ti₃C₂ MXene/GO: AgI/3D porous Ti₃C₂ MXene/graphene aerogel.

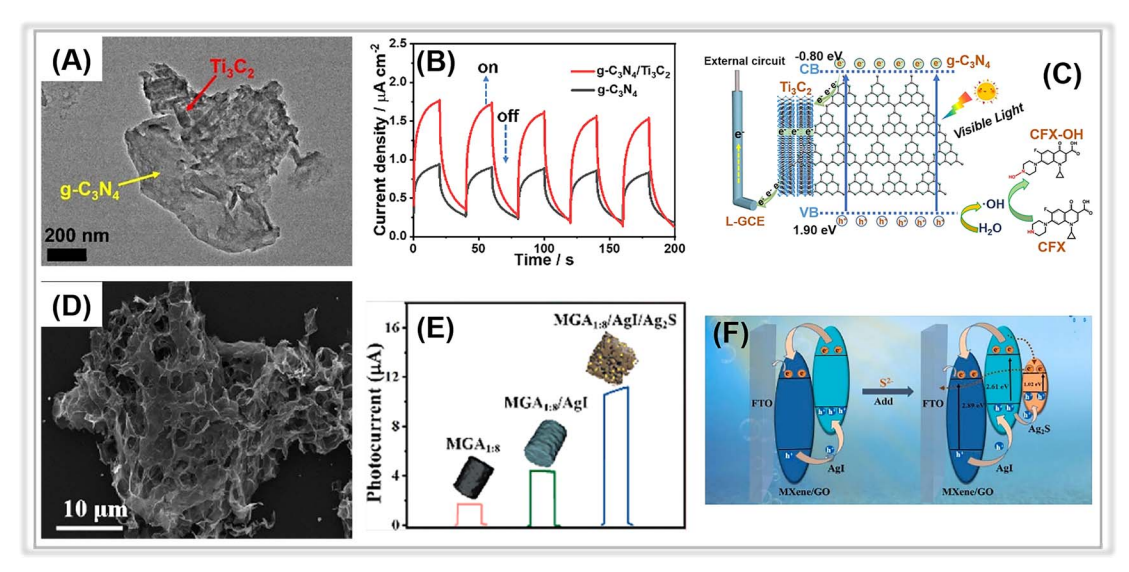


Fig. 8 (A) TEM image of the $g-C_3N_4/Ti_3C_2$ MXene composite. (B) The transient photocurrents of $g-C_3N_4$ and $g-C_3N_4/Ti_3C_2$ MXene composite. (C) The proposed PEC mechanism at the $g-C_3N_4/Ti_3C_2$ MXene composite. Adopted from ref. 196. Copyright 2021, with permission of Elsevier. (D) SEM image of Agl/ Ti_3C_2 MXene/GO composite. (E) The photocurrent responses of Ti_3C_2 MXene/GO, Agl/ Ti_3C_2 MXene/GO, and Ag₂S/Agl/ Ti_3C_2 MXene/GO composites. (F) The possible electron-transfer mechanism of the Agl/ Ti_3C_2 MXene/GO composite. Adopted from ref. 198. Copyright 2023, with permission of Elsevier.

composite surface. Thus, the improved photocurrent resulted in a wide detection range (0.1 \sim 100 nM), an ultra-low detection limit (0.03 nM), and excellent sensitivity for the corresponding PEC sensing platform.

Schottky heterojunctions have also been observed in other Ti₃C₂ MXene-containing composites. For instance, Ye et al. reported the utilization of a flower-like BiOI/2D Ti₃C₂ MXene (BiOI/Ti₃C₂) heterostructure composite as a photocathode for Lcysteine (L-Cys) PEC biosensing.203 The Schottky interaction between the two components enhanced charge transfer, resulting in a superior cathodic photocurrent signal. Similarly, a Schottky junction was also found in CdS nanoparticles and Ti₃C₂ MXene in other studies.²⁰¹ The CdS/Ti₃C₂ heterostructurebased PEC sensing platform showed a linear response for Cu²⁺ ranging from 0.1 nM to 10 µM with a LOD of 0.05 nM, attributed to significantly improved charge carrier transfer at the CdS/ Ti₃C₂ interface. In another report, Du et al. employed a wetchemical method to fabricate AgBr/Ti₃C₂ Schottky heterojunction composites for self-powered PEC sensing of chlorpyrifos (CPF).207 The synergistic effect of the Schottky heterojunction between AgBr and Ti₃C₂ MXene, combined with metal-ligand charge transfer (MLCT), promoted photogenerated charge carrier separation and transfer. The PEC sensor demonstrated excellent performance in CPF monitoring, with a linear detection range of $0.001 \sim 1$ ng L⁻¹ and a LOD of 0.33 pg L⁻¹. Recently, porous MBenes, which are respective transition metal borides, 214-218 have been applied in the areas of energy storage and electrocatalysis. Until now, there have been few reports on the application of MBenes to photoelectrochemical sensors. However, we believe that MBenes have great potential in the fabrication of PEC detection platforms.

2.6. Perspectives

In summary, over the past decade, metal oxides, MOFs, COFs, graphitic carbon nitride, and MXene have made significant advances in the construction of PEC analytical platforms for environmental contaminants. Due to their porous structure, large specific surface area and abundant active sites, PEC sensors based on photoactive porous material exhibit superior optoelectronic response. (1) Among the photoactive metal oxides, TiO2 nanotubes or nanoarrays with unique porous channels can efficiently transmit photogenerated charge pairs. PEC sensors based on TiO2 nanotubes or nanoarrays can be applied to detect heavy metal ions and organic pollutants, such as Cr(vI) and atrazine. (2) MOFs and COFs both exhibit excellent photoelectrochemical detection performance against organic pollutants. Moreover, derivatives of MOFs have demonstrated robust PEC detection activities against environmental toxic species. (3) Bulk g-C₃N₄ can be treated with a variety of methods to obtain a porous structure, including chemical exfoliation, thermal oxidation, and alkaline hydrothermal treatment. Meanwhile, the construction of 3D frameworks is another approach to obtain porous structures. A number of research works have demonstrated that porous graphitic carbon nitride-based PEC sensors exhibit outstanding detection activity in terms of ultra-low detection limit and wide linear detection range. (4) Porous MXenes characterized by high redox reactivity, superior electrical conductivity, and rich functional groups, can effectively be coupled with other materials to construct composite hybrid PEC platforms for pollutant determination. Therefore, porous materials have great potential for the fabrication of PEC sensors.

3. Applications for determining the environmental pollutants

3.1. Heavy metal ions

Heavy metal ions are highly detrimental environmental contaminants that can enter living organisms through the food chain and cause enzyme inhibition, poor antioxidant metabolism, DNA damage, and depletion of protein sulfhydryl groups. 219-221 Copper (Cu), iron (Fe), manganese (Mn), cobalt (Co), and zinc (Zn) are required for biological functions at relatively low concentrations but become toxic in excessive amounts. Low amounts of lead (Pb), mercury (Hg), chromium (Cr), cadmium (Cd), and arsenic (As) are nevertheless dangerous.222,223 The World Health Organization (WHO) has established stringent restrictions regarding the concentration of heavy metal ions in drinking water. In recent years, many efforts have been dedicated to developing porous materialbased PEC sensors for monitoring heavy metal ions. 46,167,224,225 In this section, we present a selection of relevant works on PEC detection of heavy metal ions.

3.1.1. Cr(v1). Hexavalent chromium (Cr(v1)) has been identified as one of the most toxic heavy metal ions, posing a significant threat to biological and ecological systems.²²⁶ Thus, it is critical for detecting Cr(v1) in water bodies. Several studies have been conducted to improve the PEC detection performance for Cr(v1).227 For instance, Qiao et al. constructed a NiCo-LDHs-modified TiO2 NTAs/Ti photoelectrode using anodization and electrodeposition techniques. 55 The proposed PEC sensor demonstrated a linear relationship between photocurrents and Cr(vi) concentrations ranging from 10 µM to 400 μM, with a LOD of 3.2 μM. Moreover, the sensor displayed no discernible reactions even when subjected to various interfering ions at high concentrations (e.g., Cr³⁺, Sn⁴⁺, Cd²⁺, Pb²⁺, Mn²⁺, Na⁺, and Fe²⁺), indicating its strong selectivity for Cr(v_I). More importantly, the practical application of the developed PEC sensor was examined by detecting Cr(vi) in river water, demonstrating its excellent potential in real-world scenarios. Additionally, porous graphitic carbon nitride has been employed for the construction of PEC platform for Cr(v1) detection. For instance, Fang et al. designed a formate anionincorporated graphitic carbon nitride (F-g-C₃N₄)-based PEC sensor for determining trace amounts of Cr(v1). 165 The porous Fg-C₃N₄ demonstrated enhanced photogenerated charge separation efficiency compared with bulk g-C₃N₄. Furthermore, when combined with the molecularly imprinted polymers (MIPs), F-g-C₃N₄ served as a sensing platform for Cr(v_I) determination. The resulting sensor exhibited remarkable sensitive, demonstrating a linear range from 0.01 μ g L⁻¹ to 100 μ g L⁻¹, and achieving a LOD of approximately 0.006 $\mu g L^{-1}$.

The construction of heterojunctions was another strategy to improve the PEC detection activity for Cr(vI). For instance, in 2021, Cheng *et al.* devised a quick and highly sensitive PEC sensor for determining Cr(vI) in water samples. The photoactive electrode consisted of a p-n BiOI/CN heterojunction composite. The CN nanosheets were effectively coupled to the BiOI with a needle-like petal structure. The photocurrent

density of BiOI/CN was significantly higher than that of pure CN and BiOI, suggesting that the introduction of porous CN enhanced the visible light absorption. Moreover, the BiOI/CN processed the smallest charge transfer resistance due to its unique structure, leading to increased active area and electric conductivity of the photoelectrode. Furthermore, the PEC detection performance of the composite-based electrode for Cr(v_I) was studied at various Cr(v_I) concentrations. It displayed a wide linear detection range of 0.5~190 μM with a LOD of 0.1 μM. Under visible light irradiation, the electrons in the VB of CN and BiOI were excited to their CB. Due to the Fermi level of the p-type BiOI being close to the VB and that of the n-type CN being close to the CB, electrons in the CB of the CN tended to diffuse into the BiOI, while holes in the VB were transferred from the BiOI to the CN. The electrons in CB of CN could react with Cr(v1) to convert it to harmless Cr(III). As a result, an interfacial electric field was formed between BiOI and CN, facilitating the separation of photogenerated charge pairs.

3.1.2. Hg²⁺. Another harmful heavy metal contaminant commonly found in water bodies is Hg2+. It can cause damage to the brain, kidneys, and central nervous system. EPA has defined a maximum allowable limit of 10 nM of inorganic mercury in drinking water. 228,229 Therefore, it is critical to detect it accurately. Porous MXene-based composites have been employed to construct PEC platforms for monitoring Hg^{2+} in water bodies. For instance, Xiao et al. prepared BiOBi_xI_{1-x}/Ti₃C₂ MXene Schottky heterojunction nanocomposites using an electrostatic selfassembly method.202 Porous Ti₃C₂ MXene possesses a high specific surface area, excellent electrical conductivity, and an abundance of surface chemical groups. In addition, the Schottky heterojunction of Ti₃C₂ MXene and BiOBi_xI_{1-x} significantly enhances the separation rate of photogenerated charge pairs, resulting in a higher photocurrent signal compared to BiOBi_xI_{1-x} alone. During the detection of Hg2+, an ultra-low detection limit of around 42.1 pM was obtained, ranging from 0.1 nM to 1000 nM. Moreover, this sensor has been successfully employed to determine Hg^{2^+} in environmental samples. Similarly, Jiang et al. used a BiVO₄/Ti₃C₂ MXene composite to construct a visible light-driven PEC sensor for probing Hg²⁺. 200 A single Ti₃C₂ MXene layer was coated on the BiVO₄ film. Electrochemical impendence spectroscopy measurements revealed a smaller arc diameter for the interfacial charge transfer resistance of the composite photoelectrode compared to pure BiVO₄. Further, the photocurrent signal of the composite-based electrode was higher than that of BiVO₄ (Fig. 9B). Meanwhile, the photocurrents of BiVO₄ and BiVO₄/Ti₃C₂ MXene-based electrodes increased upon the addition of glutathione (GSH) (Fig. 9A). The porous MXene, a metallike material with high conductivity, was coupled with BiVO₄ to form a Schottky junction, facilitating charge-pair separation. Thus, the performance of the PEC analysis for Hg²⁺ demonstrated a detection limit of 1.0 pM within a range of 1 pM to 2 nM.

3.1.3. Cu²⁺. Cu²⁺ is required by all living organisms. However, excessive amounts of copper can cause hepatic or renal damage, as well as gastrointestinal disturbances. Therefore, it is critical to detect Cu²⁺ concentration levels in environmental and biological samples.^{230,231} Porous material-based PEC sensors for monitoring Cu²⁺ have been investigated by

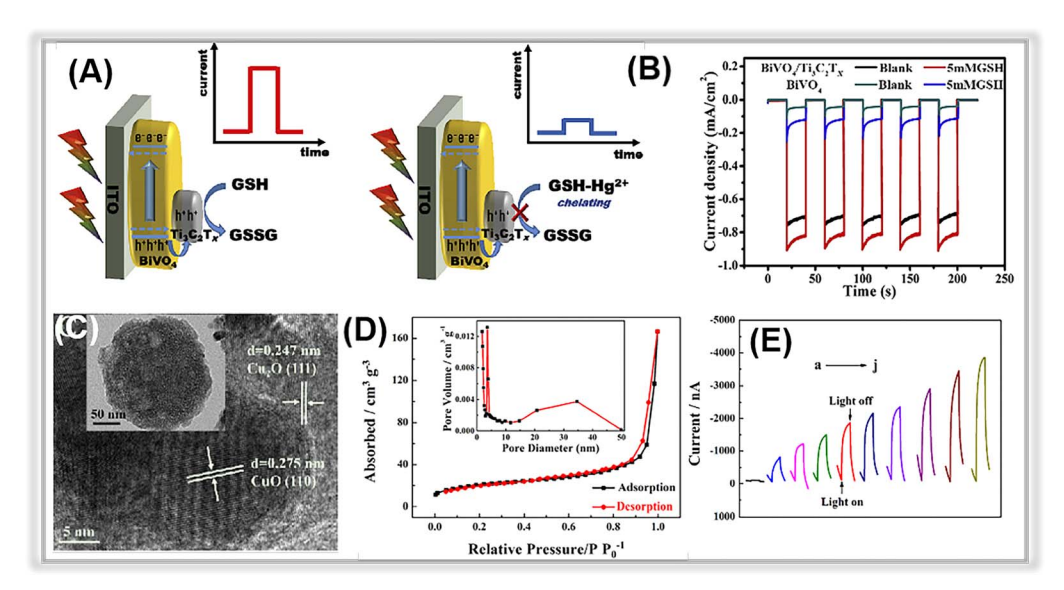


Fig. 9 (A) The mechanism of sensing Hg^{2+} with the photoelectrochemical method. (B) The photocurrent responses of $\mathrm{BiVO_4}$ and $\mathrm{Ti_3C_2}$ MXene/ $\mathrm{BiVO_4}$. Adopted from ref. 200. Copyright 2020, with permission of Elsevier. (C) TEM and HR-TEM images of $\mathrm{Cu_2O-CuO-TiO_2}$ composites. (D) Nitrogen adsorption–desorption isotherms of the $\mathrm{Cu_2O-CuO-TiO_2}$. (E) Photocurrent responses with different Pb^{2+} concentrations. Adopted from. 12 Copyright 2022, with permission of Elsevier.

several researchers. 43,73,163 For instance, in a study by Xu and coworkers, a porous graphene-analogue carbon nitride (GA-C₃N₄) was derived from the graphitic C₃N₄. 164 GA-C₃N₄ is an ideal candidate for a PEC sensor to determine Cu²⁺ due to its thin layer structure and high specific surface area. The fabricated sensor demonstrated a linear photocurrent response with varying Cu²⁺ concentrations over a wide range of $0.4\sim7.6~\mu M$.

3.1.4. Pb²⁺. Even at low concentrations, lead ions (Pb²⁺) represent a major threat to both species and human health. The United States Environmental Protection Agency (EPA) has established that the maximum allowed quantity of Pb2+ ions in drinking water is 15 ppb (72 nM),232 hence, reliable detection is critical.233-235 For example, in a recent study by Yu and coworkers, a label-free and ultrasensitive PEC biosensor was developed for the determination of Pb2+.112 The NH2-MIL-125(Ti) was synthesized via a hydrothermal method and subsequently doped with Cu. The Cu²⁺-doped-titanium-based metal-organic framework (Cu²⁺/NH₂-MIL-125(Ti)) was calcinated to create a porous Cu2O-CuO-TiO2 heterojunction composite. In Fig. 9C, the composite exhibited a disk-like morphology, and the presence of Cu2O and CuO was confirmed by HR-TEM measurements. The nitrogen adsorption-desorption isotherm of the composite was shown in Fig. 9D, revealing a specific surface area (SSA) of up to 75.1 m² g⁻¹ and an average pore size of 18.4 nm. Consequently, the porous structure and high SSA were beneficial for enhancing light absorption and facilitating the photogenerated charge transport during PEC detection. In Fig. 9E, the composite-based sensor exhibited a broad detection range of 10 fM to 1 μM and a low detection limit (6.8 fM).

3.1.5. Perspectives. In summary, significant efforts have been devoted to the fabrication of photoelectrochemical sensing platforms based on photoactive porous materials for

heavy metal ion assays. These platforms exhibited improved sensing activity, such as excellent sensitivity, an ultra-low detection limit (pM), and a wide linear range. The advantage of porous materials in the detection of heavy metal ions has been proven by the reports cited above: (1) porous material with a large surface area and abundant functional groups facilitates interaction with recognition elements or heavy metal ions; (2) fast photogenerated charge carrier separation and transfer rate within the photoactive porous materials. However, some challenges still remain with the porous material-based PEC detection sensors for heavy metal ion assays and need to be resolved: (1) some toxic heavy metal ions, such as arsenic (As⁵⁺), have not yet been monitored by porous materials-based PEC sensors; (2) despite the great potential of metal-organic frameworks for PEC detection of heavy metal ions, few works have been reported; and (3) the stability, repeatability, multiple detection, and antiinterference of heavy metal ion PEC sensors still require enhancement.

3.2. Organic pollutants

Organic pollutants found in wastewater encompass a wide range of compounds, including phenolics, antibiotics, pesticides, and toxins. These substances are extremely toxic and pose serious risks to human health. Thus, developing environmentally friendly methods for accurately determining these contaminants has become a focus of worldwide.^{236,237}

3.2.1. Phenolics. Phenols and their derivatives are known for their recalcitrance and acute toxicity. Under EPA regulations, the permissible limit for phenol in surface water is no more than 1 ppb. High concentrations of phenolic compounds can have adverse effects on human health, such as salivation and anorexia. Hence, increasing attention has been focused on detecting these phenolic species. Porous carbon nitride is an

excellent choice for developing PEC platforms for phenolic assays. For instance, Chen et al. produced a sensitive PEC detection: 0.5 pM). sensor for p-nitrotoluene (p-NT) detection based on a copper cluster-modified porous carbon nitride nanosheet composite (CNNS-Cu). 170 Under light irradiation, the Cu²⁺ cluster captures the electrons on the CB and converts them to Cu⁺. Meanwhile, the electrons excited from the VB of the CNNS are occupied by Cu²⁺, which enhances the separation and migration of photo-

generated charge pairs. Upon the introduction of p-NT, Cu^{2+} facilitates p-NT reduction via Cu2+/Cu+ redox reduction. As a result, this PEC sensor exhibits a wide linear detection range $(0.1\sim100 \mu M)$ and a low detection limit of 0.13 μM . In addition to graphitic carbon nitride with a porous structure, TiO2 nanotubes with unique pore channels have been employed in PEC applications for phenols determination. For example, Wang et al. developed a novel PEC sensor for bisphenol A detection by combining a TiO2 nanotubes/CdS heterostructure with inorganic framework molecular technology in PEC sensor analysis.78 The porous pore structures of TiO2 nanotubes favor photogenerated charge transfer, and the formation of CdS/TiO₂ heterojunctions enhances the visible light absorption and improves photoinduced charge pair separation efficiency. Moreover, the inorganic framework molecular imprinting method creates plenty of recognition sites for target analytes (BPA). Hence, the fabricated sensor demonstrated excellent PEC sensing performance (detection range: 1~100 pM, low limit

3.2.2. Antibiotics. Antibiotics are widely used in human healthcare, aquaculture, and crop growth. However, the misuse and discharge of antibiotics into the environment have raised significant concerns.239 The release of antibiotic-containing wastewater poses a severe threat to both human health and ecological systems. 14,240-242 Consequently, there is an urgent need to develop sensitive and effective methods for antibiotics detection.243-246 Recently, Liu et al. reported a simple PEC aptasensor for tracing sulfadimethoxine (SDM) based on a zinc phthalocyanine/graphitic carbon nitride composite (ZnPc/ CN).174 By modifying porous graphitic carbon nitride nanosheets with visible/near-infrared light-responsive ZnPc, ZnPc/ CN nanocomposites were created. The porous CN nanosheets not only provided abundant sites for binding ZnPc, but also facilitated transport of photogenerated charges. The assembled PEC apta-sensor exhibited a linear correlation with SDM concentration in the range of 0.1~300 nM, with a LOD of 0.03 nM. Further, it demonstrated excellent selectivity towards SDM even in the presence of familiar interferences (e.g., oxytetracycline, kanamycin, bisphenol A, and diclofenac). Similarly, using the same sensing strategy,175 a facile PEC aptasensor based on a p-type BiFeO₃/n-type porous ultrathin graphitic carbon nitride (BiFeO₃/utg-C₃N₄) was constructed

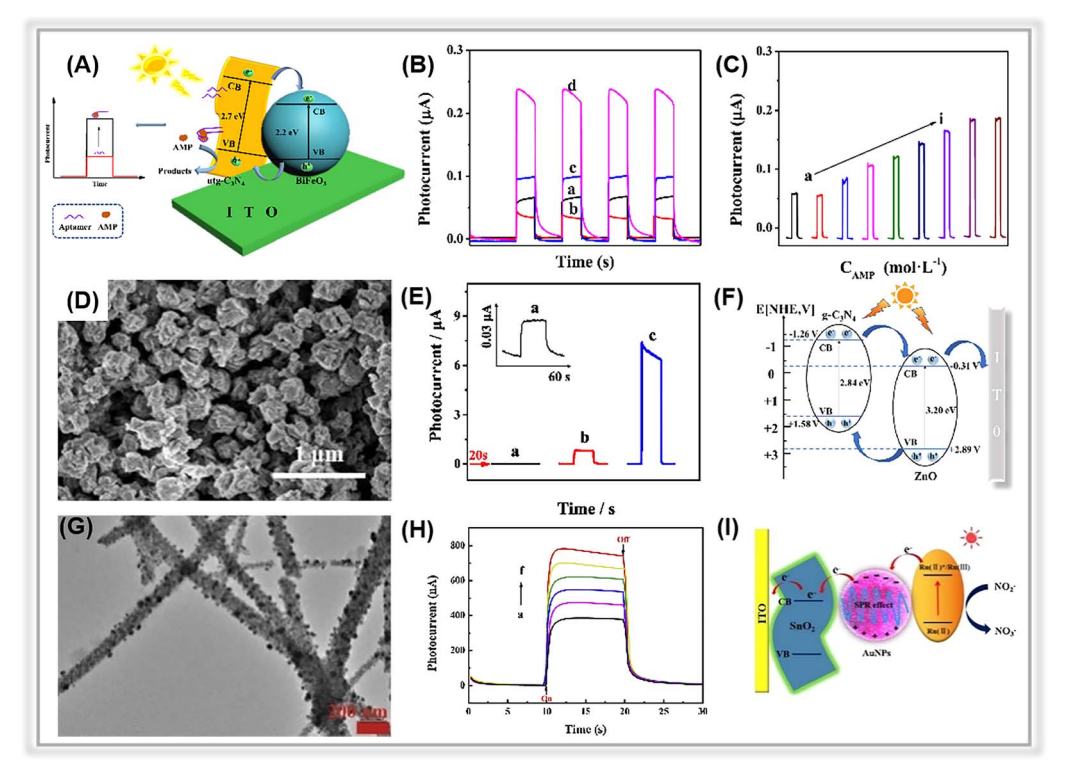


Fig. 10 (A) The illustration of the PEC ampicillin apta-sensor based on the BiFeO $_3$ /utg-C $_3$ N $_4$ composite. (B) The photocurrent signals of (a) utg- C_3N_4 , (b) $BiFeO_3$, (c) $BiFeO_3$ /bulk- C_3N_4 , and (d) $BiFeO_3$ /utg- C_3N_4 . (C) Photocurrent responses of the as-prepared apta-sensor at various ampicillin concentrations. Adopted from ref. 175. Copyright 2019, with permission of Elsevier. (D) SEM image of the ZnO/g-C₃N₄ composite. (E) The transient photocurrent responses of (a) $g-C_3N_4$, (b) ZnO, and (c) ZnO/g-C₃N₄. (F) Electron transfer mechanism for ZnO/g-C₃N₄. Adopted from ref. 117. Copyright 2023, with permission of Elsevier. (G) TEM images of SnO₂-Au NPs. (H) The photocurrent responses of SnO₂-Au NPs with different concentrations of nitrite. (I) The possible mechanism of PEC sensing nitrite. Adopted from ref. 85. Copyright 2020, with permission of Elsevier.

RSC Advances Review

(Fig. 10A). The BiFeO₃/utg-C₃N₄ composite was obtained by a simple electrostatic interaction method. The TEM image confirmed the coupling of BiFeO₃ NPs to the porous graphitic carbon nitride surface. In Fig. 10B, the composite-based electrode exhibited a significantly higher photocurrent intensity than pure BiFeO₃ and utg-C₃N₄, indicating the suppression of photogenerated charge pair recombination due to the presence of p–n heterojunction in the composite. The EIS analysis further confirmed the efficient charge separation and transfer in the BiFeO₃/utg-C₃N₄ composite-based electrodes, as they exhibited the smallest charge transfer resistance among all the electrodes. The fabricated PEC sensor was applied to ampicillin detection. As displayed in Fig. 10C, the apta-sensor achieved a relatively low LOD of 0.33 pM within a wide range from 1 pM to 1 μM.

Further, the porous graphitic carbon nitride can be combined with metal oxides derived from metal-organic frameworks to construct heterojunction composites. In 2023, Jiang et al. synthesized a MOF-derived ZnO nanopolyhedra/g-C₃N₄ composite via calcination of ZIF-8 and melamine. ¹¹⁷ The g-C₃N₄ nanosheets were covered on the ZnO surface (Fig. 10D). In Fig. 10E, the remarkable photocurrent of the ZnO/g-C₃N₄ composite-based electrodes compared to pure ZnO was attributed to the presence of heterojunctions that facilitate the separation of photogenerated electron-hole pairs. A plausible electron transfer mechanism was proposed in Fig. 10F. Due to the suitable band energy levels of ZnO and g-C₃N₄, a type-II heterojunction is formed at the contact interface of the two components. As a result, the corresponding PEC apta-sensor demonstrated an ultra-low LOD (1.49 pM) in a wide linear range spanning from 5 pM to 200 nM. Furthermore, in addition to aptamer-based PEC sensors, recognition element-free sensors have been employed for the detection of antibiotics. For instance, Yan et al. presented a non-recognition element PEC sensor using a porous nitrogen-deficient graphitic carbon nitride nanosheet (ND-g-CN) for ciprofloxacin (CIP) detection. 169 Notably, the presence of nitrogen vacancies serves as traps, effectively suppressing charge recombination, while the porous sheet structure promotes the separation and transfer of photogenerated charge carriers. Thus, the PEC sensor realized an ultra-sensitive determination of CIP (LOD: 20 ng L^{-1}).

3.2.3. Pesticides. Pesticides, even in low concentrations, can have a significant impact on the ecosystem and human health due to their high toxicity and resistance to decomposition. Therefore, extensive efforts have been made to trace these pesticides in the environment. In 2020, Qin et al. synthesized CdS nanocrystal-functionalized porous ultrathin MnO₂ nanosheet composites (CdS/MnO₂). They established a linear relationship between the concentration of organophosphorus pesticides (OPs) and photocurrent by utilizing enzymatic etching of MnO₂ nanosheets and enzyme inhibition by OPs. The constructed PEC sensor had the merits of excellent stability, a wide linear range (0.05~10 ng mL⁻¹), and outstanding sensitivity.

Different from the enzyme-based biosensor, a self-powered PEC apta-sensor was constructed for diazinon (DZN) detection based on porous graphitic carbon nitride (CN).¹⁸⁰ In this PEC apta-sensor, sulfur-doped h-BN (S-BN) was combined with the

porous graphitic carbon nitride (CN), and Au nanoparticles with localized surface plasmon resonance (LSPR) effect acted as bridges to create a Z-scheme heterojunction, thereby enhancing the separation efficiency of photogenerated charge pairs. The proposed PEC sensor exhibited the benefits of a low detection limit (6.8 pM), a broad linear detection range (0.01 \sim 10 000 nM), and excellent selectivity for DZN detection.

3.2.4. Toxins. Toxins are harmful compounds produced by living cells or organisms, including microcystin-LR (MC-LR), ochratoxin A (OTA), and aflatoxin B1 (AFB1).250 Therefore, the development of simple and sensitive methods for detecting such toxins is critical. Recently, Li et al. constructed a photoelectrochemical sensor for MC-LR detection, employing bismuth/two-dimensional graphitic carbon nitride/ deoxyribonucleic acid (BiVO₄/2D-C₃N₄/DNA) aptamer system. 186 The porous graphitic carbon nitride nanosheets were modified onto the surface of the BiVO₄ film photoelectrode. The coupling of 2D-C₃N₄ with BiVO₄ formed a type-II heterojunction, enhancing the transfer capacity of photogenerated electron-hole via an internal electric field effect. Additionally, 2D-C₃N₄ effectively absorbed the DNA aptamer probe owing to its large area of π - π bonds. Thus, the sensor achieved a LOD of $0.04~{\rm pg}~{\rm L}^{-1}$ within the range of $0.5~{\rm pg}~{\rm L}^{-1}{\sim}10~{\rm \mu g}~{\rm L}^{-1}$. Apart from the conventional type-II heterojunction, the porous g-C₃N₄ has been combined with various semiconductors and electron transfer mediators (e.g., Ag, Au, and Pt) to construct Z-scheme heterojunction composites. For instance, Tang et al. developed a self-powered photoelectrochemical apta-sensor for MC-LR determination based on a Z-scheme CoO/Au/g-C₃N₄ heterojunction composite.185 In this composite, both CoO and Au nanoparticles were well anchored to the surface of the porous g-C₃N₄. The well-matched energy bands between CoO and g-C₃N₄, along with the presence of Au NPs as electron transfer mediators, significantly improved the separation efficiency of photogenerated charge pairs. Thus, the detection limit for this sensor was lowered to 0.01 pM over a wide range from 0.1 pM to 10 nM.

3.2.5. Perspectives. Overall, PEC sensors based on photoactive porous materials hold significant promise for the sensitive and selective detection of organic environmental pollutants. Metal oxides (such as TiO2), metal-organic frameworks, covalent organic frameworks, graphitic carbon nitride, and MXene all exhibit huge potential for detecting various types of toxic organic contaminants, including phenolics, antibiotics, pesticides, toxins, and dyes. These materials demonstrate robust photoelectrochemical detection performance with high sensitivity and excellent selectivity. Nevertheless, there are still some challenges in this field: (1) most of reported PEC sensors for organic environmental pollutants assays still rely on the target as the electron donor during the detection procedures, which results in relatively low interference in complex samples. Therefore, there is a need for the development of novel photoactive porous materials that can directly interact with organic analytes. (2) The anti-fouling properties of photoactive porous materials need improvement due to the adsorption of organic molecules and their derivatives on the surface of these materials.

Review **RSC Advances**

3.3. Non-metal ion pollutants

Apart from heavy metal ions and organic pollutants, there is growing concern regarding non-metal ion pollutants, including nitrites, sulfides, and cyanides.251 Recently, several works have focused on the PEC detection of these non-metal ion pollutants in the environment. 252,253 In 2017, Su et al. described a novel PEC sensor for sulfide detection using Cu₂O-decorated TiO₂ nanotubes.84 The p-n heterojunction in the porous Cu2O-TiO2 heterostructure effectively suppressed the recombination of photogenerated charge pairs, leading to enhanced photocurrent response. The detection of sulfide by this sensor displayed a wide linear range from 1 μ M to 300 μ M, and the LOD was 0.6 μM. Furthermore, it has been successfully employed for accurate sulfide monitoring in tap and lake water, achieving outstanding recoveries ranging from 99.2% to 103%.

In addition to the detection of toxic sulfides in water bodies, the PEC sensing platform has also been utilized for tracing nitrides. For instance, Luo et al. constructed a porous threedimensional (3D) network of SnO2 nanofibers on an ITO substrate using an electrospinning technique, followed by the electrodeposition of gold nanoparticles (Au NPs).85 The presence of porous SnO₂ nanofibers with a 3D network structure was beneficial for the photogenerated charge pair separation and transfer (as shown in Fig. 10G). Moreover, Au NPs with the LSPR effect suppressed recombination of electron-hole pairs. By utilizing the photosensitizer-Ru(bpy)₃²⁻, the photocurrent response was further increased. As illustrated in Fig. 10I, under the 473 nm light irradiation, the SnO2 could not be excited, whereas Au NPs and Ru(bpy)₃²⁻ were both excited. Ru²⁺ was excited into unstable Ru2+*, and the electrons were transferred to the Au or SnO2 nanofibers. These electrons were then transferred into the conduction band of SnO2 with the aid of Au NPs in the surface plasma state. The Ru²⁺ ions were converted to Ru³⁺ ions, which then reacted with NO₂⁻ to form NO₃⁻ and Ru²⁺ ions. As a result, a linear relationship between photocurrent and NO₂ concentration was established. Under optimized test conditions, the fabricated sensor demonstrated a wide linear range from 1 to 10 000 nM with a LOD of 0.48 nM (Fig. 10H).

Conclusion and outlook

Photoelectrochemical detection has emerged as a promising analytical method for tracing environmental pollutants due to its distinct advantages, including cost-effectiveness, rapid response, minimal background noise, and high sensitivity. Crucially, photoactive materials, which significantly influence the monitoring activity of PEC sensors, are key components of these sensing systems. In particular, porous materials have garnered considerable interest in the design and fabrication of photoelectrochemical sensing platforms due to their unique properties, such as a high surface area, tunable pore sizes, and an abundance of functional groups. In this review, we summarize recent advances in photoactive porous materialbased photoelectrochemical sensors and their applications in monitoring environmental contaminants in water bodies based on a substantial body of research. We introduce and categorize

typical porous materials into five groups: metal oxides, metalorganic frameworks, covalent organic frameworks, graphitic carbon nitride, and MXene. Additionally, we separately discuss their applications in detecting heavy metal ions, organic pollutants, and non-metal ion pollutants.

Most importantly, the structural effects of porous materials on the photoelectrochemical detection performance (sensitivity, detection limits, selectivity, and stability) of associated sensors have been discussed in detail in several representative works. Based on the comparison of numerous references, the structural effects of porous materials on PEC detection activity can be summarized into the following critical points: (1) enhancement of the light absorption ability through the multiple reflection of light in pores, improving the light harvesting capability; (2) acceleration of the photoinduced electron-hole pair separation and transfer through the unique porous structures with considerable small pores, shortening the separation and migration route and suppressing charge pair recombination; (3) improvement of the surface charge transfer rate, porous materials with the high surface area provide abundant active sites for chemical reactions and facilitate the detection of species capture. From the aforementioned advantages of porous materials for the construction of photoelectrochemical sensing platforms, we strongly confirm the remarkable potential of porous materials for environmental pollutant detection.

Despite excellent advances and rapid progress in the field of photoelectrochemical sensors based on porous materials for environmental toxic species assays, some fundamental issues and emerging challenges remain:

- (1) Even though much effort has been devoted to the application of porous materials in PEC sensors for environmental hazard detection, only a small portion of the vast family of porous materials has been used to fabricate PEC sensing platforms. Meanwhile, some porous materials are only preliminary to PEC sensing applications for highly toxic species, such as photoactive COFs. Therefore, it still has huge potential for exploitation. Furthermore, relatively few porous materials have been used for heavy metal ion assays, only metal oxides and graphitic carbon nitride. Some toxic heavy metal ions, such as arsenic, have not been detected by porous material-based PEC sensors.
- (2) Most studies of porous materials focus on the energy level structure and neglect the unique porous structures, e.g., pore diameter and surface area. In addition, the effect of the porous structure on the photoinduced charge transfer and separation efficiency needs to be explored more. More importantly, although the photoelectric coordination of the detection mechanism based on the porous materials has been explained in several works, they only prefer to discuss the photocurrent signal generation mechanism in terms of the classical semiconductor theory and the consideration of the structural effects on the detection mechanism are somewhat insufficient. More attention should be paid to it for future studies, as porous structures favor trapping of probe species and an abundance of functional groups provides more active sites for the occurrence of relevant redox reactions. Moreover, the stability of PEC

sensors based on porous materials requires more attention due to the fragile nature of porous structures and multiple assembly

processes.

(3) The application of porous materials to PEC sensing is primarily at the laboratory stage. For practical applications, it still suffers from several shortcomings, such as relatively low reliability and reproducibility. Moreover, real samples may contain multiple environmental hazards, thus requiring multiplexing sensing capabilities for PEC sensors based on porous materials. In the field of environmental sample detection, integrating PEC detection methods with flexible electrodes, such as conductive polymers and carbon paper, is highly recommended. Flexible electrodes support the miniaturization and development of wearable and smart devices. PEC detection strategies should be combined with intelligent technologies to enable real-time and in situ detection, while still emphasizing the stability, convenience, and operability of integrated detection devices. Additionally, there are currently few commercial PEC sensing devices on the market, which hinders the development of PEC sensing methods. Therefore, future research should focus more on the fabrication of PEC-related equipment. With the help of smart technologies and the potential for commercial benefits, the current limitations of PEC sensing can be resolved.

Data availability

RSC Advances

The data that support the findings of this study are available from the corresponding author upon reasonable request.

Author contributions

Shiben Liu, conceptualization, paper writing; Jinhua Zhan, analysis of article structure and error proofreading; Bin Cai, collecting data and providing financial support. Shiben Liu's writing, first draft preparation. Jinhua Zhan and Bin Cai's writing, review and proofreading.

Conflicts of interest

The authors declare no conflict of interest.

Acknowledgements

This project was supported by the National Natural Science Foundation of China (52201262), Guangdong Basic and Applied Basic Research Foundation (2021A1515110920), Natural Science Foundation of Shandong Province (ZR2022QE001), Program Taishan Scholars of Shandong Province (tsqn202211042), and Shandong Postdoctoral Science Foundation (SDCX-ZG-202303013).

References

- 1 H. Xu, Y. Jia, Z. Sun, J. Su, Q. S. Liu, Q. Zhou and G. Jiang, Eco-Environ. Health, 2022, 1, 31-45.
- 2 B. Wang and Y. Wang, Sci. Total Environ., 2022, 831, 154906.

- Saravanan, P. S. Kumar, R. V. Hemavathy, S. Jeevanantham, P. Harikumar, G. Priyanka and D. R. A. Devakirubai, Sci. Total Environ., 2022, 812, 152456.
- 4 P. Chowdhary, A. Raj and R. N. Bharagava, Chemosphere, 2018, 194, 229-246.
- 5 O. Surucu, Mater. Today Chem., 2022, 23, 100639.
- 6 C. Xu, M. He, B. Chen and B. Hu, Talanta, 2022, 245, 123470.
- 7 J. Borrull, A. Colom, J. Fabregas, F. Borrull and E. Pocurull, J. Chromatogr. A, 2020, 1621, 461090.
- 8 H. Zheng, J. Hong, X. Luo, S. Li, M. Wang, B. Yang and M. Wang, Microchem. J., 2019, 145, 806-812.
- 9 M. Soylak, M. Alasaad and Ö. Özalp, Microchem. J., 2022, 178, 107329.
- 10 V. Vogiazi, A. de la Cruz, S. Mishra, V. Shanov, W. R. Heineman and D. D. Dionysiou, ACS Sens., 2019, 4,
- 11 Z. Li and M. Zhu, Chem. Commun., 2020, 56, 14541-14552.
- 12 C. Zhu, D. Liu, Y. Li, X. Shen, L. Li, Y. Liu and T. You, Curr. Opin. Electrochem., 2019, 17, 47-55.
- 13 L. Ge, Q. Liu, N. Hao and W. Kun, J. Mater. Chem. B, 2019, 7, 7283-7300.
- 14 Q. Liu, H. Zhang, H. Jiang, P. Yang, L. Luo, Q. Niu and T. You, Biosens. Bioelectron., 2022, 216, 114634.
- 15 Y. Zhou, H. Yin, W. W. Zhao and S. Ai, Coord. Chem. Rev., 2020, 424, 213519.
- 16 W. W. Zhao, J. J. Xu and H. Y. Chen, Chem. Soc. Rev., 2015, 44, 729-741.
- 17 L. Yang, S. Zhang, X. Liu, Y. Tang, Y. Zhou and D. K. Y. Wong, J. Mater. Chem. B, 2020, 8, 7880-7893.
- 18 Z. Qiu and D. Tang, J. Mater. Chem. B, 2020, 8, 2541-2561.
- 19 Y. Zang, J. Lei and H. Ju, Biosens. Bioelectron., 2017, 96, 8-
- 20 M. Azriouil, M. Matrouf, F. E. Ettadili, F. Laghrib, A. Farahi, S. Sagrane, M. Bakasse, S. Lahrich and M. A. El Mhammedi, Food Chem. Toxicol., 2022, 168, 113378.
- 21 C. Huang, L. Zhang, Y. Zhu, Z. Zhang, Y. Liu, C. Liu, S. Ge and J. Yu, Anal. Chem., 2022, 94, 8075-8084.
- 22 J. Zhao, C. Fu, C. Huang, S. Zhang, F. Wang, Y. Zhang, L. Zhang, S. Ge and J. Yu, Chem. Eng. J., 2021, 406, 126892.
- 23 S. Wang, F. Wang, C. Fu, Y. Sun, J. Zhao, N. Li, Y. Liu, S. Ge and J. Yu, Anal. Chem., 2020, 92, 7604-7611.
- 24 I. Ibrahim, H. N. Lim, R. Mohd Zawawi, A. Ahmad Tajudin, Y. H. Ng, H. Guo and N. M. Huang, J. Mater. Chem. B, 2018, 6, 4551-4568.
- 25 H. Wang, B. Zhang, Y. Tang, C. Wang, F. Zhao and B. Zeng, TrAC, Trends Anal. Chem., 2020, 131, 116020.
- 26 W. Ma, D. Han, M. Zhou, H. Sun, L. Wang, X. Dong and L. Niu, Chem. Sci., 2014, 5, 3946-3951.
- 27 M. Song, H. Sun, J. Yu, Y. Wang, M. Li, M. Liu and G. Zhao, ACS Appl. Mater. Interfaces, 2021, 13, 37212-37222.
- 28 M. Lv, W. Zhou, H. Tavakoli, C. Bautista, J. Xia, Z. Wang and X. Li, Biosens. Bioelectron., 2021, 176, 112947.
- 29 B. Peng, L. Tang, G. Zeng, Y. Zhou, Y. Zhang, B. Long, S. Fang, S. Chen and J. Yu, Curr. Anal. Chem., 2018, 14, 4–12.
- 30 W. W. Zhao, J. J. Xu and H. Y. Chen, TrAC, Trends Anal. Chem., 2016, 82, 307-315.

31 Y. Zheng, Y. Zhou, X. Cui, H. Yin and S. Ai, *Mater. Today Chem.*, 2022, **24**, 100878.

- 32 J. H. Zhu, M. Wang, L. H. Tu, A. J. Wang, X. Luo, L. P. Mei, T. Zhao and J. J. Feng, *Sens. Actuators, B*, 2021, 347, 130553.
- 33 J. Shu and D. Tang, Anal. Chem., 2020, 92, 363-377.
- 34 Z. Qiu, J. Shu, J. Liu and D. Tang, Anal. Chem., 2019, 91, 1260–1268.
- 35 K. Zhang, S. Lv and D. Tang, Analyst, 2019, 144, 5389-5393.
- 36 J. Shu, Z. Qiu, Q. Zhou, Y. Lin, M. Lu and D. Tang, *Anal. Chem.*, 2016, **88**, 2958–2966.
- 37 Y. Zhou, H. Yin and S. Ai, Coord. Chem. Rev., 2021, 447, 214156.
- 38 A. Y. S. Tan, H. T. A. Awan, F. Cheng, M. Zhang, M. T. T. Tan, S. Manickam, M. Khalid and K. Muthoosamy, *Chem. Eng. J.*, 2024, 482, 148774.
- 39 X. Ma, J. Kang, Y. Wu, C. Pang, S. Li, J. Li, Y. Xiong, J. Luo, M. Wang and Z. Xu, *TrAC*, *Trends Anal. Chem.*, 2022, 157, 116793.
- 40 R. Yadav, T. Baskaran, A. Kaiprathu, M. Ahmed, S. V. Bhosale, S. Joseph, A. H. Al-Muhtaseb, G. Singh, A. Sakthivel and A. Vinu, *Chem.-Asian J.*, 2020, 15, 2588– 2621.
- 41 B. R. Thompson, T. S. Horozov, S. D. Stoyanov and V. N. Paunov, *J. Mater. Chem. A*, 2019, 7, 8030–8049.
- 42 Z. Li, Y. Li, S. Chen, Q. Zha and M. Zhu, *Chem. Eng. J.*, 2023, **460**, 141657.
- 43 J. Du, Y. Fan, X. Gan, X. Dang and H. Zhao, *Electrochim. Acta*, 2020, **330**, 135336.
- 44 H. Xiong, Y. Dong, D. Liu, R. Long, T. Kong and Y. Xiong, *J. Phys. Chem. Lett.*, 2022, **13**, 1272–1282.
- 45 Y. Chen, L. Li, Q. Xu, W. Chen, Y. Dong, J. Fan and D. Ma, *Sol. RRL*, 2021, **5**, 2000541.
- 46 X. Dong, D. Liu, X. Meng and T. You, *Anal. Sci.*, 2022, **38**, 459–481.
- 47 L. Li, J. Chen, C. Xiao, Y. Luo, N. Zhong, Q. Xie, H. Chang, D. Zhong, Y. Xu, M. Zhao and Q. Liao, *Chin. Chem. Lett.*, 2022, 34, 107904.
- 48 Q. Zhou and D. Tang, TrAC, Trends Anal. Chem., 2020, 124, 115814.
- 49 Y. T. Xu, S. Y. Yu, Y. C. Zhu, G. C. Fan, D. M. Han, P. Qu and W. W. Zhao, *TrAC, Trends Anal. Chem.*, 2019, **114**, 81–88.
- 50 B. Wang, J. T. Cao and Y. M. Liu, *Analyst*, 2020, **145**, 1121–1128.
- 51 K. Yan, P. Karthick Kannan, D. Doonyapisut, K. Wu, C. H. Chung and J. J. A. F. M. Zhang, *Adv. Funct. Mater.*, 2021, 31, 2008227.
- 52 A. Huang, Y. He, Y. Zhou, Y. Zhou, Y. Yang, J. Zhang, L. Luo, Q. Mao, D. Hou and J. Yang, J. Mater. Sci., 2018, 54, 949–973.
- 53 H. Peng, W. Xiong, Z. Yang, J. Tong, M. Jia, Y. Xiang, S. Sun and Z. Xu, *Chem. Eng. J.*, 2023, **457**, 141317.
- 54 Y. Wang, M. Zu, X. Zhou, H. Lin, F. Peng and S. Zhang, *Chem. Eng. J.*, 2020, **381**, 122605.
- 55 J. Qiao, Y. Wang, Q. Liang, S. Dong, Z. Zeng and S. Shao, *ACS Appl. Nano Mater.*, 2022, 5, 5535–5543.
- 56 X. Sun, C. Gao, L. Zhang, M. Yan, J. Yu and S. Ge, *Sens. Actuators*, *B*, 2017, 251, 1–8.

- 57 J. Tian, Y. Li, J. Dong, M. Huang and J. Lu, *Biosens. Bioelectron.*, 2018, **110**, 1-7.
- 58 M. Jia, Z. Yang, H. Xu, P. Song, W. Xiong, J. Cao, Y. Zhang, Y. Xiang, J. Hu, C. Zhou, Y. Yang and W. Wang, *Chem. Eng. J.*, 2020, 388, 124388.
- 59 W. Dong, B. Wang, Y. Xue and G. Jie, *Sens. Actuators, B*, 2023, 393, 134293.
- 60 B. Zhang, H. Meng, X. Wang, J. Li, H. Chang and W. Wei, *Sens. Actuators, B*, 2018, 255, 2531–2537.
- 61 B. Zhang, H. Wang, H. Ye, B. Xu, F. Zhao and B. Zeng, *Sens. Actuators*, *B*, 2018, 273, 1435–1441.
- 62 X. Ouyang, C. Feng, L. Tang, X. Zhu, B. Peng, X. Fan, Y. Liao, Z. Zhou and Z. Zhang, *Biosens. Bioelectron.*, 2022, 197, 113734.
- 63 S. Adhikari, S. Selvaraj and D. H. Kim, *Appl. Catal.*, B, 2019, 244, 11–24.
- 64 Q. Cai, T. Yin, Y. Ye, G. Jie and H. Zhou, *Anal. Chem.*, 2022, **94**, 5814–5822.
- 65 N. Zhang, Y. Li, G. Zhao, J. Feng, Y. Li, Y. Wang, D. Zhang and Q. Wei, *Talanta*, 2023, 253, 124048.
- 66 F. Tavella, C. Ampelli, S. G. Leonardi and G. Neri, *Sensors*, 2018, **18**, 3566.
- 67 L. Fan, G. Liang, C. Zhang, L. Fan, W. Yan, Y. Guo, S. Shuang, Y. Bi, F. Li and C. Dong, *J. Hazard. Mater.*, 2021, 409, 124894.
- 68 J. Wu, P. Ou, Y. Lin, X. Tan, F. Wei, Y. Mi, S. Liu and K. Huang, J. Electroanal. Chem., 2022, **911**, 116220.
- 69 H. Wu, Z. Zheng, Y. Tang, N. M. Huang, R. Amal, H. N. Lim and Y. H. Ng, Sustainable Mater. Technol., 2018, 18, e00075.
- 70 S. Velmurugan, C. K. Y. T, J. Ching Juan and J. N. Chen, *J. Colloid Interface Sci.*, 2021, **596**, 108–118.
- 71 J. Jana, T. S. K. Sharma, J. S. Chung, W. M. Choi and S. H. Hur, J. Alloys Compd., 2023, 946, 169395.
- 72 Y. Liang, B. Kong, A. Zhu, Z. Wang and Y. Tian, *Chem. Commun.*, 2012, 48, 245–247.
- 73 J. Tang, J. Li, Y. Zhang, B. Kong, Yiliguma, Y. Wang, Y. Quan, H. Cheng, A. M. Al-Enizi, X. Gong and G. Zheng, *Anal. Chem.*, 2015, 87, 6703–6708.
- 74 R. Wang, X. Pang, H. Zhang, P. Gao, B. Du, H. Ma and Q. Wei, *Anal. Methods*, 2015, 7, 5406–5411.
- 75 K. Wang, N. Sun, X. Li, R. Zhang, G. Zu, J. Wang and R. Pei, *Anal. Methods*, 2015, 7, 9340–9346.
- 76 T. Tran.T., J. Li, H. Feng, J. Cai, L. Yuan, N. Wang and Q. Cai, *Sens. Actuators, B*, 2014, **190**, 745–751.
- 77 Y. Qin, Y. Wu, G. Chen, L. Jiao, L. Hu, W. Gu and C. Zhu, *Anal. Chim. Acta*, 2020, **1130**, 100–106.
- 78 L. Wang, H. Zhang, H. Shi, B. Jin, X. Qin, G. Wang, K. Li, T. Zhang and H. Zhang, *Anal. Methods*, 2021, 13, 2857–2864.
- 79 B. Zhang, L. Lu, F. Huang and Z. Lin, *Anal. Chim. Acta*, 2015, 887, 59–66.
- 80 F. Han, Z. Song, M. H. Nawaz, M. Dai, D. Han, L. Han, Y. Fan, J. Xu, D. Han and L. Niu, *Anal. Chem.*, 2019, 91, 10657–10662.
- 81 X. Qin, Q. Wang, L. Geng, X. Shu and Y. Wang, *Talanta*, 2019, **197**, 28–35.
- 82 C. Wang, H. Wang, M. Zhang, B. Zeng and F. Zhao, *Sens. Actuators*, *B*, 2021, 339, 129900.

83 M. Liu, J. Yu, X. Ding and G. Zhao, Electroanalysis, 2016, 28,

RSC Advances

- 161–168. 84 Y. Su, S. Yang, W. Liu, L. Qiao, J. Yan, Y. Liu, S. Zhang and
- Y. Fang, *Microchim. Acta*, 2017, **184**, 4065–4072. 85 J. Luo, Y. Jiang, X. Guo, Y. Ying, Y. Wen, P. Lin, Y. Sun,
- 85 J. Luo, Y. Jiang, X. Guo, Y. Ying, Y. Wen, P. Lin, Y. Sun, H. Yang and Y. Wu, *Sens. Actuators, B*, 2020, 309.
- 86 S. Hu, Y. Wei, J. Wang and Y. Yu, *Anal. Chim. Acta*, 2021, **1178**, 338793.
- 87 Y. Shi, Y. Zou, M. S. Khan, M. Zhang, J. Yan, X. Zheng, W. Wang and Z. Xie, *J. Mater. Chem. C*, 2023, **11**, 3692–3709.
- 88 P. Samanta, A. V. Desai, S. Let and S. K. Ghosh, *ACS Sustain. Chem. Eng.*, 2019, 7, 7456–7478.
- 89 Y. Hua, D. Kukkar, R. J. C. Brown and K. H. Kim, *Crit. Rev. Environ. Sci. Technol.*, 2022, 53, 258–289.
- 90 R. Gupta, F. Rahi Alhachami, I. Khalid, H. S. Majdi, N. Nisar, Y. Mohamed Hasan, R. Sivaraman, R. M. Romero Parra, Z. I. Al Mashhadani and Y. Fakri Mustafa, Crit. Rev. Anal. Chem., 2022, 1–22.
- 91 H. Du, T. Yin, J. Wang and G. Jie, *Anal. Chem.*, 2023, 95, 7053–7061.
- 92 X. Zhang, T. Yan, T. Wu, Y. Feng, M. Sun, L. Yan, B. Du and Q. Wei, *Biosens. Bioelectron.*, 2019, **135**, 88–94.
- 93 H. Dai, X. Yuan, L. Jiang, H. Wang, J. Zhang, J. Zhang and T. Xiong, *Coord. Chem. Rev.*, 2021, 441, 213985.
- 94 Z. Mo, D. Tai, H. Zhang and A. Shahab, *Chem. Eng. J.*, 2022, 443, 136320.
- 95 F. Z. Chen, Y. Gao, Y.-J. Li, W. Li, X. Y. Wu, D. M. Han and W. W. Zhao, *Sens. Actuators*, *B*, 2022, **361**, 136651.
- 96 L. Hanna, C. L. Long, X. Zhang and J. V. Lockard, *Chem. Commun.*, 2020, **56**, 11597–11600.
- 97 Y. Yang, W. Yan, X. Wang, L. Yu, J. Zhang, B. Bai, C. Guo and S. Fan, *Biosens. Bioelectron.*, 2021, 177, 113000.
- 98 R. Feng, X. Zhang, X. Xue, Y. Xu, H. Ding, T. Yan, L. Yan and Q. Wei, ACS Appl. Bio Mater., 2021, 4, 7186–7194.
- 99 Y. Wu, K. Lu, F. Pei, Y. Yan, S. Feng, Q. Hao, M. Xia and W. Lei, *Talanta*, 2022, **248**, 123617.
- 100 Y. Cao, L. Wang, C. Wang, X. Hu, Y. Liu and G. Wang, *Electrochim. Acta*, 2019, **317**, 341–347.
- 101 W. Dong, Z. Li, W. Wen, S. Feng, Y. Zhang and G. Wen, *RSC Adv.*, 2021, **11**, 28320–28325.
- 102 W. Dong, Z. Li, W. Wen, B. Liu and G. Wen, *ACS Appl. Mater. Interfaces*, 2021, **13**, 57497–57504.
- 103 L. Zhang, L. Feng, P. Li, X. Chen, J. Jiang, S. Zhang, C. Zhang, A. Zhang, G. Chen and H. Wang, *Chem. Eng. J.*, 2020, 395, 125702.
- 104 J. Liu, X. Yu, Y. Xu, Y. Zhao and D. Li, *Inorg. Chem.*, 2021, **60**, 19044–19052.
- 105 Y. Wang, D. Jin, X. Zhang, J. Zhao and X. Hun, *Mikrochim. Acta*, 2022, **189**, 193.
- 106 J. Xiong, W. Tan, J. Cai, K. Lu and X. Mo, *Int. J. Electrochem. Sci.*, 2022, **17**, 22048.
- 107 P. W. Gao, Y. Z. Shen, C. Ma, Q. Xu and X. Y. Hu, *Analyst*, 2021, **146**, 6178–6186.
- 108 M. Peng, G. Guan, H. Deng, B. Han, C. Tian, J. Zhuang, Y. Xu, W. Liu and Z. Lin, *Environ. Sci.: Nano*, 2019, 6, 207– 215.

- 109 J. Kang, X. Ma, Y. Wu, C. Pang, S. Li, J. Li, Y. Xiong, J. Luo, M. Wang and Z. Xu, *Mikrochim. Acta*, 2022, **189**, 383.
- 110 J. Gao, Y. Chen, W. Ji, Z. Gao and J. Zhang, *Analyst*, 2019, **144**, 6617–6624.
- 111 W. Li, L. Xu, X. Zhang, Z. Ding, X. Xu, X. Cai, Y. Wang, C. Li and D. Sun, *Sens. Actuators, B*, 2023, 378, 133153.
- 112 Q. Yu, Y. Fu, K. Xiao, X. Zhang, C. Du and J. Chen, *Anal. Chim. Acta*, 2022, **1195**, 339456.
- 113 D. Zheng, M. Chen, Y. Chen and W. Gao, *Anal. Chim. Acta*, 2022, **1212**, 339913.
- 114 Z. Zhang, L. Huang, S. Sheng, C. Jiang and Y. Wang, Sens. Actuators, B, 2021, 343.
- 115 Y. Cao, L. Wang, C. Wang, D. Su, Y. Liu and X. Hu, *Mikrochim. Acta*, 2019, **186**, 481.
- 116 S. Velmurugan, T. C. K. Yang, S. W. Chen and J.-N. Chen, *J. Environ. Chem. Eng.*, 2021, **9**, 106169.
- 117 H. Jiang, Q. Liu, H. Zhang, P. Yang and T. You, *J. Colloid Interface Sci.*, 2023, **632**, 35–43.
- 118 J. Peng, J. Yang, B. Chen, S. Zeng, D. Zheng, Y. Chen and W. Gao, *Biosens. Bioelectron.*, 2021, 175, 112873.
- 119 X. Zhang, J. Peng, Y. Ding, D. Zheng, Y. Lin, Y. Chen and W. Gao, *Sens. Actuators, B*, 2020, **306**, 127552.
- 120 Y. Feng, T. Yan, T. Wu, N. Zhang, Q. Yang, M. Sun, L. Yan, B. Du and Q. Wei, Sens. Actuators, B, 2019, 298, 126817.
- 121 T. Yan, X. Zhang, X. Ren, Y. Lu, J. Li, M. Sun, L. Yan, Q. Wei and H. Ju, *Sens. Actuators, B*, 2020, 320, 128387.
- 122 T. Yan, H. Ding, R. Feng, R. Yuan, Y. Zhao, M. Sun, L. Yan and Q. Wei, *ACS Appl. Mater. Interfaces*, 2022, **14**, 25308–25316.
- 123 J. Tan, B. Peng, L. Tang, G. Zeng, Y. Lu, J. Wang, X. Ouyang, X. Zhu, Y. Chen and H. Feng, *Anal. Chem.*, 2020, **92**, 13073– 13083.
- 124 C. Zhao, L. Zhang, Q. Wang, L. Zhang, P. Zhu, J. Yu and Y. Zhang, ACS Appl. Mater. Interfaces, 2021, 13, 20397–20404.
- 125 C. Wang, N. Liu, X. Liu, Y. Tian, X. Zhai, X. Chen and B. Hou, *ACS Appl. Nano Mater.*, 2021, **4**, 8801–8812.
- 126 S. Zhang, K. Chen, L. Zhu, M. Xu, Y. Song, Z. Zhang and M. Du, *Dalton Trans.*, 2021, **50**, 14285–14295.
- 127 Y. Yang, H. Wei, X. Wang, D. Sun, L. Yu, B. Bai, X. Jing, S. Qin and H. Qian, *Biosens. Bioelectron.*, 2023, 223, 115017.
- 128 X. Liu, D. Huang, C. Lai, G. Zeng, L. Qin, H. Wang, H. Yi, B. Li, S. Liu, M. Zhang, R. Deng, Y. Fu, L. Li, W. Xue and S. Chen, *Chem. Soc. Rev.*, 2019, 48, 5266–5302.
- 129 J. Liu, J. Wang, Y. Wang and Y. Wang, *J. Polym. Sci.*, 2022, 1–24.
- 130 S. Kandambeth, K. Dey and R. Banerjee, *J. Am. Chem. Soc.*, 2019, **141**, 1807–1822.
- 131 K. Geng, T. He, R. Liu, S. Dalapati, K. T. Tan, Z. Li, S. Tao, Y. Gong, Q. Jiang and D. Jiang, *Chem. Rev.*, 2020, **120**, 8814– 8933.
- 132 X. Yan, H. Li, T. Yin, G. Jie and H. Zhou, *Biosens. Bioelectron.*, 2022, **217**, 114694.
- 133 T. Liu, L. Cui, H. Zhao and X. Zhang, ACS Appl. Mater. Interfaces, 2020, 12, 47090–47098.
- 134 K. Xiao, R. Zhu, C. Du, X. Zhang and J. Chen, *Sens. Actuators*, *B*, 2023, **380**, 133403.

- 135 N. Li, C. Wang, L. Chen, C. Ye and Y. Peng, Molecules, 2022, 27, 6732.
- 136 M. Wang, G. Liang, M. Wang, M. Hu, L. Zhu, Z. Li, Z. Zhang, L. He and M. Du, Chem. Eng. J., 2022, 448, 137779.
- 137 Y. Gao, J. Zhang, X. Zhang, J. Li, R. Zhang and W. Song, Anal. Chem., 2021, 93, 8647-8655.
- 138 S. Wang, X. Xu, Y. Yue, K. Yu, Q. Shui, N. Huang and H. Chen, Small Struct., 2020, 1, 2000021.
- 139 Z. Xu, X. Cui, Y. Li, Y. Li, Z. Si and Q. Duan, Appl. Surf. Sci., 2023, 613, 155966.
- 140 T. Yan, G. Zhang, K. Yu, H. Chai, M. Tian, L. Qu, H. Dong and X. Zhang, Chem. Eng. J., 2023, 455, 104779.
- 141 D. Feng, P. Huang, Y. Miao, A. Liang, X. Wang, B. Tang, H. Hou, M. Ren, S. Gao, L. Geng and A. Luo, Sens. Actuators, B, 2022, 368, 132121.
- 142 Y. Liu, L. Zhong, S. Zhang, J. Wang and Z. Liu, Sens. Actuators, B, 2022, 354, 131204.
- 143 B. Dong, X. Zhang, L. Cao, X. Jiang and F. Wang, J. Mater. Chem. C, 2023, 11, 2074-2081.
- 144 H. Zhao, R. Su, L. Teng, Q. Tian, F. Han, H. Li, Z. Cao, R. Xie, G. Li, X. Liu and Z. Liu, Nanoscale, 2022, 14, 1653-
- 145 Q. Wang, X. Sun, C. Liu, C. Wang, W. Zhao, Z. Zhu, S. Ma and S. Zhang, Front. Bioeng. Biotechnol., 2023, 11, 1164805.
- 146 W. Y. Geng, H. Zhang, Y. H. Luo, X. G. Zhu, A. D. Xie, J. Wang and D. E. Zhang, Microporous Mesoporous Mater., 2021, 323, 111186.
- 147 M. Xu, K. Chen, L. Zhu, S. Zhang, M. Wang, L. He, Z. Zhang and M. Du, Langmuir, 2021, 37, 13479-13492.
- 148 X. Wang, K. Maeda, A. Thomas, K. Takanabe, G. Xin, J. M. Carlsson, K. Domen and M. Antonietti, Nat. Mater., 2009, 8, 76-80.
- 149 X. Huo, H. Yi, Y. Fu, Z. An, L. Qin, X. Liu, B. Li, S. Liu, L. Li, M. Zhang, F. Xu, G. Zeng and C. Lai, Energy Environ. Sci., 2021, 8, 1835-1862.
- 150 H. Li, Q. Cai, Y. Xue, G. Jie and H. Zhou, Sens. Actuators, B, 2023, 391, 134062.
- 151 T. S. K. Sharma, A. Ganguly, A. Santhan and K. Y. Hwa, ACS Appl. Nano Mater., 2022, 5, 5208-5222.
- 152 L. Xu, H. Li, P. Yan, J. Xia, J. Qiu, Q. Xu, S. Zhang, H. Li and S. Yuan, J. Colloid Interface Sci., 2016, 483, 241-248.
- 153 Y. Liu, K. Yan and J. Zhang, ACS Appl. Mater. Interfaces, 2015, 8, 28255-28264.
- 154 L. Xu, S. Ling, H. Li, P. Yan, J. Xia, J. Qiu, K. Wang, H. Li and S. Yuan, Sens. Actuators, B, 2017, 240, 308-314.
- 155 S. S. Low, Z. Chen, Y. Li, Y. Lu and Q. Liu, TrAC, Trends Anal. Chem., 2021, 145, 116454.
- 156 Q. W. Chen, C. Yuan and C. Y. Zhai, Chin. Chem. Lett., 2022, 33, 983-986.
- 157 F. K. Kessler, Y. Zheng, D. Schwarz, C. Merschjann, W. Schnick, X. Wang and M. J. Bojdys, Nat. Rev. Mater., 2017, 2, 17030.
- 158 Y. Li, X. Li, H. Zhang and Q. Xiang, Nanoscale Horiz., 2020, 5, 765-786.
- 159 X. Gao, J. Feng, D. Su, Y. Ma, G. Wang, H. Ma and J. Zhang, Nano Energy, 2019, 59, 598-609.

- 160 H. J. Li, B. W. Sun, L. Sui, D. J. Qian and M. Chen, Phys. Chem. Chem. Phys., 2015, 17, 3309-3315.
- 161 J. Zhang, Y. Chen and X. Wang, Energy Environ. Sci., 2015, 8, 3092-3108.
- 162 B. Peng, L. Tang, G. Zeng, S. Fang, X. Ouyang, B. Long, Y. Zhou, Y. Deng, Y. Liu and J. Wang, Biosens. Bioelectron., 2018, 121, 19-26.
- 163 D. Liang, X. Liang, Z. Zhang, H. Wang, N. Zhang, J. Wang and X. Qiu, Microchem. J., 2020, 156, 104922.
- 164 H. Xu, J. Yan, X. She, L. Xu, J. Xia, Y. Xu, Y. Song, L. Huang and H. Li, Nanoscale, 2014, 6, 1406-1415.
- 165 T. Fang, X. Yang, L. Zhang and J. Gong, J. Hazard. Mater., 2016, 312, 106-113.
- 166 D. Cheng, H. Wu, C. Feng, Y. Zhang, Y. Ding and H. Mei, J. Alloys Compd., 2021, 882, 160690.
- 167 Z. Li, W. Dong, X. Du, G. Wen and X. Fan, Microchem. J., 2020, 152, 104259.
- 168 J. Hu, Z. Li, C. Zhai, L. Zeng and M. Zhu, Anal. Chim. Acta, 2021, 1183, 338951.
- 169 P. Yan, J. Dong, Z. Mo, L. Xu, J. Qian, J. Xia, J. Zhang and H. Li, Biosens. Bioelectron., 2020, 148, 111802.
- 170 L. Chen, Z. Li, Q. Xiao, M. Li, Y. Xu and X. Qiu, Appl. Catal., A, 2023, 649, 118964.
- 171 Y. Xu, Z. Wen, T. Wang, M. Zhang, C. Ding, Y. Guo, D. Jiang and K. Wang, Biosens. Bioelectron., 2020, 166, 112453.
- 172 Y. Xu, D. Jiang, M. Zhang, Z. Zhang, J. Qian, N. Hao, C. Ding and K. Wang, Sens. Actuators, B, 2020, 316, 128142.
- 173 Z. Zhang, B. Peng, X. Ouyang, X. Zhu, L. Chen, X. Fan, Z. Zhou, J. Wang and L. Tang, Sens. Actuators, B, 2022, 368, 132144.
- 174 Q. Liu, T. Shi, Y. Cheng, Z. Wen, C. Ding, Y. Li and K. Wang, J. Hazard. Mater., 2021, 406, 124749.
- 175 L. Ge, Y. Xu, L. Ding, F. You, Q. Liu and K. Wang, Biosens. Bioelectron., 2019, 124-125, 33-39.
- 176 L. Xu, P. Yan, H. Li, S. Ling, J. Xia, Q. Xu, J. Qiu and H. Li, RSC Adv., 2017, 7, 7929-7935.
- 177 L. Yang, Z. Zhao, J. Hu, H. Wang, J. Dong, X. Wan, Z. Cai and M. Li, Electroanalysis, 2020, 32, 1651-1658.
- 178 W. Gong, J. Zou, S. Zhang, X. Zhou and J. Jiang, Electroanalysis, 2016, 28, 227-234.
- 179 M. Yang, Y. Jia, Y. Chen, P. Yan, L. Xu, J. Qian, F. Chen and H. Li, J. Environ. Chem. Eng., 2022, 10, 107208.
- 180 J. Tan, B. Peng, L. Tang, C. Feng, J. Wang, J. Yu, X. Ouyang and X. Zhu, Biosens. Bioelectron., 2019, 142, 111546.
- 181 Z. Qi, P. Yan, J. Qian, L. Zhu, H. Li and L. Xu, Sens. Actuators, B, 2023, 387, 133792.
- 182 B. Peng, Y. Lu, J. Luo, Z. Zhang, X. Zhu, L. Tang, L. Wang, Y. Deng, X. Ouyang, J. Tan and J. Wang, J. Hazard. Mater., 2021, 401, 123395.
- 183 S. Feng, X. Wei, L. Zhong and J. Li, Electroanalysis, 2018, 30, 320-327.
- 184 J. Wang, B. Yang, S. Li, B. Yan, H. Xu, K. Zhang, Y. Shi, C. Zhai and Y. Du, J. Colloid Interface Sci., 2017, 506, 329-337.
- 185 L. Tang, X. Ouyang, B. Peng, G. Zeng, Y. Zhu, J. Yu, C. Feng, S. Fang, X. Zhu and J. Tan, Nanoscale, 2019, 11, 12198-12209.

RSC Advances Review

- 186 Y. Li, Y. Bu, F. Jiang, X. Dai and J. P. Ao, Biosens. Bioelectron., 2020, 150, 111903.
- 187 H. Nie, M. Ou, Q. Zhong, S. Zhang and L. Yu, J. Hazard. Mater., 2015, 300, 598-606.
- 188 H. Yu, R. Shi, Y. Zhao, T. Bian, Y. Zhao, C. Zhou, G. I. N. Waterhouse, L. Z. Wu, C. H. Tung and T. Zhang, Adv. Mater., 2017, 29, 1605148.
- 189 R. Cao, H. Yang, S. Zhang and X. Xu, Appl. Catal. B: Environ., 2019, 258, 117997.
- 190 X. Chen, R. Shi, Q. Chen, Z. Zhang, W. Jiang, Y. Zhu and T. Zhang, Nano Energy, 2019, 59, 644-650.
- 191 Z. Chen, M. Asif, R. Wang, Y. Li, X. Zeng, W. Yao, Y. Sun and K. Liao, Chem. Rec., 2022, 22, e202100261.
- 192 X. Wu, P. Ma, Y. Sun, F. Du, D. Song and G. Xu, Electroanalysis, 2021, 33, 1827-1851.
- 193 Y. Pei, X. Zhang, Z. Hui, J. Zhou, X. Huang, G. Sun and W. Huang, ACS Nano, 2021, 15, 3996-4017.
- 194 D. Jiang, Y. Zhang, X. Du, L. Zhang, X. Shan, W. Wang, H. Shiigi and Z. Chen, Chem. Commun., 2023, 59, 1185-
- 195 N. H. Solangi, N. M. Mubarak, R. R. Karri, S. A. Mazari and A. S. Jatoi, Environ. Res., 2023, 222, 115279.
- 196 C. Yuan, Z. He, Q. Chen, X. Wang, C. Zhai and M. Zhu, Appl. Surf. Sci., 2021, 539, 148241.
- 197 Y. Zhou, K. Maleski, B. Anasori, J. O. Thostenson, Y. Pang, Y. Feng, K. Zeng, C. B. Parker, S. Zauscher, Y. Gogotsi, J. T. Glass and C. Cao, ACS Nano, 2020, 14, 3576-3586.
- 198 Q. Zhang, C. Wang, Y. Tian, Y. Liu, F. You, K. Wang, J. Wei, L. Long and J. Qian, Anal. Chim. Acta, 2023, 1245, 340845.
- 199 Y. Tian, C. Wang, Q. Zhang, H. Cui, Y. Liu, K. Wang, J. Wei, L. Long and J. Qian, Sens. Actuators, B, 2023, 382, 133496.
- 200 Q. Jiang, H. Wang, X. Wei, Y. Wu, W. Gu, L. Hu and C. Zhu, Anal. Chim. Acta, 2020, 1119, 11-17.
- 201 C. Ye, F. Xu, F. Ullah and M. Wang, Anal. Bioanal. Chem., 2022, 414, 3571-3580.
- 202 W. Xiao, W. Xu, W. Huang, Y. Zhou, Z. Jin, X. Wei and J. Li, ACS Appl. Nano Mater., 2022, 5, 18168-18177.
- 203 C. Ye, Z. Wu, K. Ma, Z. Xia, J. Pan, M. Wang and C. Ye, J. Alloys Compd., 2021, 859, 157787.
- 204 Y. Chen, X. Li, G. Cai, M. Li and D. Tang, Electrochem. Commun., 2021, 125, 106897.
- 205 L. Ling, C. Yuan, Q. Xu, T. Li, M. Zhu and C. Zhai, Surf. Interfaces, 2023, 36, 102483.
- 206 F. You, Z. Wen, R. Yuan, L. Ding, J. Wei, J. Qian, L. Long and K. Wang, J. Electroanal. Chem., 2022, 914, 116285.
- 207 X. Du, W. Du, J. Sun and D. Jiang, Food Chem., 2022, 385, 132731.
- 208 F. You, J. Wei, Y. Cheng, Z. Wen, C. Ding, N. Hao and K. Wang, J. Hazard. Mater., 2021, 414, 125539.
- 209 C. Chen, X. Zhou, Z. Wang, J. Han and S. Chen, Anal. Chim. Acta, 2022, 1216, 339943.
- 210 Y. Zhang, X. Du, M. Wei, X. Shan, W. Wang, D. Jiang, H. Shiigi and Z. Chen, Anal. Chim. Acta, 2023, 1238, 340645.
- 211 Y. Jin, Y. Luan, Z. Wu, W. Wen, X. Zhang and S. Wang, Anal. Chem., 2021, 93, 13204-13211.

212 Y. Sun, X. Meng, Y. Dall'Agnese, C. Dall'Agnese, S. Duan, Y. Gao, G. Chen and X. F. Wang, Nano-Micro Lett., 2019, 11, 79.

- 213 M. Tahir, A. Ali Khan, S. Tasleem, R. Mansoor and W. K. Fan, Energy Fuels, 2021, 35, 10374-10404.
- 214 V. G. Nair, M. Birowska, D. Bury, M. Jakubczak, A. Rosenkranz and A. M. Jastrzebska, Adv. Mater., 2022, 34, e2108840.
- 215 M. Jakubczak, A. Szuplewska, A. Rozmysłowska Wojciechowska, A. Rosenkranz and A. M. Jastrzębska, Adv. Funct. Mater., 2021, 31, 2103048.
- 216 M. Khazaei, J. Wang, M. Estili, A. Ranjbar, S. Suehara, M. Arai, K. Esfarjani and S. Yunoki, Nanoscale, 2019, 11, 11305-11314.
- 217 B. Zhang, J. Zhou and Z. Sun, J. Mater. Chem. A, 2022, 10, 15865-15880.
- 218 A. Sharma, V. S. Rangra and A. Thakur, J. Mater. Sci., 2022, 57, 12738-12751.
- 219 C. Venkateswara Raju, C. Hwan Cho, G. Mohana Rani, V. Manju, R. Umapathi, Y. Suk Huh and J. Pil Park, Coord. Chem. Rev., 2023, 476, 214920.
- 220 R. Sharma, N. F. Suhendra, S. H. Jung and H. i. Lee, Chem. Eng. J., 2023, 451, 138506.
- 221 R. Sharma, S. N. Chavan and H. i. Lee, Sens. Actuators, B, 2023, 396, 134625.
- 222 W. W. Zhao, J. J. Xu and H. Y. Chen, Analyst, 2016, 141, 4262-4271.
- 223 X. Gan, H. Zhao, R. Schirhagl and X. Quan, Mikrochim. Acta, 2018, 185, 478.
- 224 R. Ahmad, N. Tripathy, A. Khosla, M. Khan, P. Mishra, W. A. Ansari, M. A. Syed and Y. B. Hahn, J. Electrochem. Soc., 2020, 167, 037519.
- 225 M. Xu, X. Wang and X. Liu, J. Agric. Food Chem., 2022, 70, 11468-11480.
- 226 S. Prasad, K. K. Yadav, S. Kumar, N. Gupta, M. M. S. Cabral Pinto, S. Rezania, N. Radwan and J. Alam, J. Environ. Manage., 2021, 285, 112174.
- 227 K. Dashtian, M. Ghaedi and S. Hajati, Biosens. Bioelectron., 2019, 132, 105-114.
- 228 W. L. Cui, Z. H. Zhang, L. Wang, J. Qu and J. Y. Wang, Spectrochim. Acta, Part A, 2022, 267, 120516.
- 229 Y. Wang, Y. Wang, F. Wang, H. Chi, G. Zhao, Y. Zhang, T. Li and Q. Wei, J. Colloid Interface Sci., 2022, 606, 510-517.
- 230 J. Wang, Y. Pan, L. Jiang, M. Liu, F. Liu, M. Jia, J. Li and Y. Lai, ACS Appl. Mater. Interfaces, 2019, 11, 37541-37549.
- 231 K. Wang, J. Yang, X. Yang, Q. Guo and G. Nie, Microchem. J., 2022, 182, 107952.
- 232 EPA, Office of Water, Washington, DC, USA, 2009.
- 233 Y. Niu, G. Luo, H. Xie, Y. Zhuang, X. Wu, G. Li and W. Sun, Mikrochim. Acta, 2019, 186, 826.
- 234 L. Meng, M. Liu, K. Xiao, X. Zhang, C. Du and J. Chen, Chem. Commun., 2020, 56, 8261-8264.
- 235 Y. Wang, G. Zhao, G. Zhang, Y. Zhang, H. Wang, W. Cao, T. Li and Q. Wei, Sens. Actuators, B, 2020, 319, 128313.
- 236 B. M. da Costa Filho, A. C. Duarte and T. A. P. Rocha-Santos, Trends Environ. Anal. Chem., 2022, 33, e00154.

237 Z. Li, H. Zhang, Q. Zha, J. Li and M. Zhu, *Catalysts*, 2023, **13**, 91.

- 238 R. Gusain, K. Gupta, P. Joshi and O. P. Khatri, *Adv. Colloid Interface Sci.*, 2019, 272, 102009.
- 239 C. Liu, B. Li, M. Liu and S. Mao, Sens. Actuators, B, 2022, 369, 132383.
- 240 J. Wang and R. Zhuan, Sci. Total Environ., 2020, 701, 135023.
- 241 P. Yan, D. Jiang, Y. Tian, L. Xu, J. Qian, H. Li, J. Xia and H. Li, *Biosens. Bioelectron.*, 2018, **111**, 74–81.
- 242 T. S. K. Sharma and K. Y. Hwa, Chem. Eng. J., 2022, 439, 135591.
- 243 X. Liu, P. Liu, Y. Tang, L. Yang, L. Li, Z. Qi, D. Li and D. K. Y. Wong, *Biosens. Bioelectron.*, 2018, **112**, 193–201.
- 244 X. Qin, L. Geng, Q. Wang and Y. Wang, *Mikrochim. Acta*, 2019, **186**, 430.
- 245 Y. Wang, F. Bian, X. Qin and Q. Wang, *Mikrochim. Acta*, 2018, **185**, 161.

- 246 Y. Chen, Y. Wang, P. Yan, Q. Ouyang, J. Dong, J. Qian, J. Chen, L. Xu and H. Li, *Anal. Chim. Acta*, 2020, 1125, 299–307.
- 247 D. Vaya and P. K. Surolia, *Environ. Technol. Innovation*, 2020, **20**, 101128.
- 248 H. Wang, D. Liang, Y. Xu, X. Liang, X. Qiu and Z. Lin, *Environ. Sci.: Nano*, 2021, **8**, 773–783.
- 249 Q. Liu, Y. Yin, N. Hao, J. Qian, L. Li, T. You, H. Mao and K. Wang, Sens. Actuators, B, 2018, 260, 1034–1042.
- 250 Z. Lei, P. Lei, J. Guo and Z. Wang, *Talanta*, 2022, 248, 123607.
- 251 R. Sharma, N. F. Suhendra and H. i. Lee, *Sens. Actuators, B*, 2023, **382**, 133570.
- 252 Q. Li, J. Yao, Y. Jiang, X. Guo, Y. Ying, Y. Wen, X. Liu, Y. Wu, H. Yang and C. Le, *I. Electroanal. Chem.*, 2022, **917**, 116412.
- 253 P. Teng, X. Wen, Z. Liu, J. Zhang, Y. Zhang, N. Copner, J. Yang, K. Li, M. Bowkett, D. Gao, L. Yuan and X. Zhu, *Opt. Commun.*, 2022, 502, 127436.